

# Populating the Galaxy with pulsars I: stellar & binary evolution

Paul D. Kiel<sup>1\*</sup>, Jarrod R. Hurley<sup>1</sup>, Matthew Bailes<sup>1</sup> and James R. Murray<sup>1</sup>

<sup>1</sup> *Centre for Astrophysics and Supercomputing, Swinburne University of Technology, Hawthorn, Victoria, 3122, Australia*

Accepted xxx. Received xxx; in original form xxx

## ABSTRACT

The computation of theoretical pulsar populations has been a major component of pulsar studies since the 1970s. However, the majority of pulsar population synthesis has only regarded isolated pulsar evolution. Those that have examined pulsar evolution within binary systems tend to either treat binary evolution poorly or evolve the pulsar population in an ad-hoc manner. Thus no complete and direct comparison with observations of the pulsar population within the Galactic disk has been possible to date. Described here is the first component of what will be a complete synthetic pulsar population survey code. This component is used to evolve both isolated and binary pulsars. Synthetic observational surveys can then be performed on this population for a variety of radio telescopes. The final tool used for completing this work will be a code comprised of three components: stellar/binary evolution, Galactic kinematics and survey selection effects. Results provided here support the need for further (apparent) pulsar magnetic field decay during accretion, while they conversely suggest the need for a re-evaluation of the assumed *typical* MSP formation process. Results also focus on reproducing the observed  $P\dot{P}$  diagram for Galactic pulsars and how this precludes short timescales for standard pulsar exponential magnetic field decay. Finally, comparisons of bulk pulsar population characteristics are made to observations displaying the predictive power of this code, while we also show that under standard binary evolutionary assumption binary pulsars may accrete much mass.

**Key words:** binaries: close – stars: evolution – stars: pulsar – stars: neutron – Galaxy: stellar content

## 1 INTRODUCTION

Since the tentative suggestion that neutron stars (NSs) form from violent supernova (SN) events (Baade & Zwicky 1934a, 1934b) and the discovery of pulsars by Hewish et al. (1968) the number of observed pulsars has risen dramatically. Surveys for radio pulsars have discovered over 1500 objects including a rich harvest of binary and millisecond pulsars (Manchester et al. 2005; Burgay et al. 2006). Precision timing of pulsars in binary systems has not only allowed precise tests of theories of relativistic gravity (e.g. van Straten et al. 2001), but also given insights into their masses and the nature of the binary systems they inhabit (for example Verbiest et al. 2007; Bell, Bailes & Bessell, 1993). Of the first 300 or so pulsars to be discovered, only 3 were members of binary systems, despite the progenitor population having an extremely high binary fraction ( $> 50\%$ ; Duquennoy & Mayor, 1991). This paucity of binary pulsars was an important clue about the origin and evolution of pulsars. Clearly

something about pulsar generation was contributing to the disruption of binary systems. We now believe that the supernovae in which pulsars are produced impart significant kicks to the pulsars, that make their survival prospects within binary systems bleak.

Today, there are well over 100 binary pulsars known, and their spin periods and inferred magnetic field strengths offer the opportunity to attempt models of binary evolution and pulsar spin-up that explain their distribution in the pulsar magnetic field-spin period ( $B_s$ - $P$ ) diagram. To do this properly, one should take models of an initial population of zero-age main-sequence (ZAMS) single stars and binaries, trace the binary and stellar evolution, including neutron star spin-up effects, calculate their Galactic trajectories and initial distribution in the Galaxy, and then perform synthetic surveys assuming a pulsar luminosity and beaming function. This is what we wish to achieve. The large number of assumptions that we require to complete this effort caution against the absolute predictive power of such a model. For instance, it is easy to demonstrate that trying to use such a model to predict something like the merger rate of NS-

\* E-mail: pkiel@astro.swin.edu.au (PDK)

black hole (BH), or double pulsars/NSs based solely on a consideration of the total number and mass distributions of un-evolved ZAMS binaries would be folly. However, the relative numbers of two or more populations can often only depend upon relatively few model assumptions (as shown in HTP02; Belczynski, Kalogera & Bulik 2002; O’Shaughnessy et al. 2008). With enough observables in time we might hope to build up a self-consistent theory of binary and pulsar evolution. This paper, the first in a series, aims to address the above suggested binary and stellar pulsar evolution population synthesis component. Later work will combine this product with the kinematic and selection effect components, facilitating direct comparison of theory with observations. Therefore this paper is only a first step towards such a complete description but one that, as we will show, can already constrain models of neutron star magnetic field evolution and spin-up.

As alluded to above, observations of pulsars take the form of spin measurements – both the spin period  $P$  and spin period derivative  $\dot{P}$  – in which the surface magnetic field  $B_s$  and characteristic age of the pulsars are inferred (details are discussed when we introduce our model of pulsar evolution). It is instructive to plot  $\dot{P}$  vs  $P$  (hereafter  $P\dot{P}$ ) and  $B_s$  vs  $P$  diagrams and any theoretical model must be able to reproduce these if it is to be successful. In Figure 1 we show the  $B_s$  vs  $P$  diagram of  $\sim 1400$  pulsars taken from the ATNF Pulsar Catalogue<sup>1</sup> (Manchester et al. 2005). We see three distinct regions of the parameter space being populated. A large island of relatively slow spinning pulsars with high surface magnetic fields (and thus high  $\dot{P}$ s) is joined via a thin bridge of pulsars to another, smaller, island of relatively rapid rotators with low magnetic fields.

The present theoretical explanation for the distinct groups of observed pulsars is rotating magnetic neutron stars that are either isolated or reside in a binary system (see Wheeler 1966; Pacini 1967; Gold, 1968; Ostriker & Gunn 1969; Gunn & Ostriker 1970; Goldreich & Julian 1969, van den Heuvel 1984, Colpi et al. 2001; Bhattacharya 2002; Harding & Lai 2006). It is those NSs that evolve within a binary system that may attain the low surface magnetic fields and low rotational periods, i.e. rapid rotators, as mentioned above. The double pulsar binary J0737-3039A & B (Burgay et al. 2003; Lorimer 2004; Lyne et al. 2004; Dewi & van den Heuvel 2004) shows the distinction between rapid rotators and slow rotators clearly. Here we have a binary system consisting of a millisecond pulsar (MSP:  $P = 22.7$  ms and  $B_s = 7 \times 10^9$  G) and its ‘standard’ pulsar companion ( $P = 2.77$  s and  $B_s = 6 \times 10^{12}$  G). Although it seems likely that it is the process of accretion onto the NS that induces NS magnetic field decay (or apparent magnetic field decay) this evolutionary phase is still highly contentious and theories abound on how the decay may occur. One such theoretical argument is of accretion-induced field decay via ohmic dissipation of the accreting NSs crustal currents. This is due to the heating of the crust which in turn increases the resistance in the crust (Konar & Bhattacharya 1997, 1999a, 1999b; Geppert & Urpin 1994; Urpin & Geppert 1995; Romani 1990; Urpin, Geppert & Konenkov 1997). An alternative explanation of accretion-induced field decay

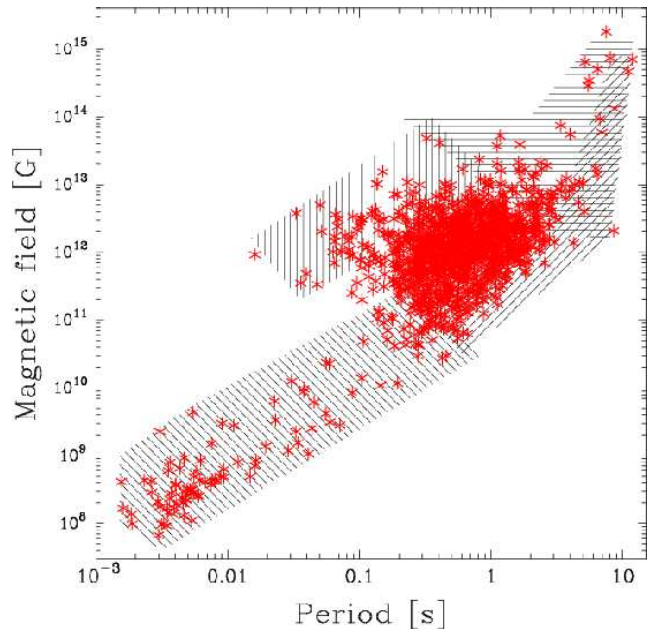


**Figure 1.** Magnetic field vs spin period of observed pulsars within the Galaxy (stars, including some within globular clusters). The observations are overlaid with a cartoon depiction of the reason for the particulars of the pulsar parameter space distribution. The area covered by vertical bars primarily arises from the canonical pulsar birth properties and spin-down due to magneto-rotational energy losses. The horizontal barred regions are formed for the most part by deviation of pulsar birth properties from the average values from whence pulsar spin-down evolution commences. Forward leaning horizontal bars depict the region in which a luminosity law or loss of obliquity of beam direction (or a combination of these) induces a decrease of numbers in the observed population. The final observed pulsar region arises from binary evolution, although a number of these systems are isolated it is possible they were formed in binaries which disrupted due to the explosion or ablation of the secondary star.

consists of screening or burying the magnetic field with the accreted material (Lovelace, Romanova & Bisnovatyi-Kogan 2005; Konar & Choudhuri 2004; Choudhuri & Konar 2002; Cumming, Zweibel & Bildsten 2001; Melatos & Phinney 2001; Bisnovatyi-Kogan & Komberg 1974; Taam & van den Heuvel 1986). While yet another argument considers vortex-fluxoid (neutron-proton) interactions. Here the neutron vortices latch on and then drag the proton vortices (which bear the magnetic field) radially, the radial direction is induced by either spin-up (inwards) or spin-down (outwards) of the NS (Jahan-Miri 2000; Muslimov & Tsygan 1985; Ruderman 1991a, b & c).

Below is a general overview of pulsar evolutionary paths. A greater level of detail is given within the very informative reviews presented by Colpi et al. (2001), Bhattacharya (2002), Choudhuri & Konar (2004), Payne & Melatos (2004), Harding & Lai (2006) and references therein. There are a number of possible binary and stellar evolutionary paths one can conceive that allow the formation of a pulsar. If the end product is an isolated ‘standard’ pulsar, the star may have always been isolated and evolved from a massive enough progenitor star (mass greater than  $\sim 10 M_\odot$ ) with no evolutionary perturbations from outside influences. However, it may have been that the progenitor

<sup>1</sup> <http://www.atnf.csiro.au/research/pulsar/psrcat/>

pulsar was bound in an orbit and depending on the orbital parameters when the NS formed, mass loss and the velocity kick during the asymmetric SN event (Shklovskii 1970) could contrive to disrupt the binary, allowing us to observe a solitary pulsar. Alternatively, if the secondary star was also massive (but originally the less massive of the two stars) disruption may occur in a second SN event. The creation of a millisecond (re-cycled; Alpar et al. 1982) pulsar requires the accretion of material onto the surface of the NS at some point during its lifetime. For this to occur the primary star is first required to form a NS and the binary must survive the associated SN event. Then, some time later, the secondary star evolves to overflow its Roche-lobe and initiate a steady mass transfer phase. Any accretion of the donated material onto the NS will increase its spin angular momentum, thus spinning up the pulsar, potentially to a millisecond spin period. The companion of the resultant MSP will typically be a low-mass main sequence star, a white dwarf (WD: a MSP-WD binary) or another pulsar. Formation of a double pulsar binary is problematic because if more than half of the systems mass is lost in the second SN event the binary will be disrupted. This is unless a kick is directed toward the vicinity of the companion MSP with just the right magnitude to overcome the energy change owing to mass loss but not too strong as to disrupt the binary. If instead the binary is disrupted by the SN then there would be both a solitary ‘standard’ pulsar and a single MSP. One other suggested method for producing a single millisecond pulsar is for the donor star to be evaporated or ablated by the extremely active pulsar radiation (which may be modelled in the form of a wind). The pulsar is then said to be a black widow pulsar (van Paradijs et al. 1988).

As mentioned above, the theories of pulsar evolution can be tested in a statistical manner by comparing observations to population synthesis results. This theoretical approach has been adopted previously for pulsars and other stellar systems (some examples are: Dewey & Cordes 1987; Bailes 1989; Rathnasree 1993; Possenti et al. 1998; Portegies Zwart & Yungelson 1998; Possenti et al. 1999; Willems & Kolb 2002; O’Shaughnessy et al. 2005; Kiel & Hurley 2006; Dai, Liu & Li 2006; Story, Gonthier & Harding 2007 and numerous works based on STARTRACK, presented in Belczynski et al. 2008). The level of detail in the population synthesis calculations varies, along with the methodologies the authors implemented. For example, Bailes (1989) considered pulsar selection effects in some detail, however, only roughly considered binary evolutionary phases and the method in which this affects pulsar evolution. Willems & Kolb (2002) considered NS populations and how these affect the resultant NS populations, however, they were not able to directly compare with observations as no selection effects were modelled. In a slightly different approach (empirically based) Kim, Kalogera & Lorimer (2003) estimated the merger rate (via gravitational waves) of double NS (DNS) binaries within the Galaxy by selecting the physical *observable* DNS pulsar properties from appropriate distribution functions for many pulsars and weighting these against the observed Galactic disk DNS pulsars PSR B1913+16 and PSR B1534+12. Taking into account selection effects of the pulsar population for large scale surveys and producing many pulsar models they were able to give confidence levels for their merger rate estimates. In comparison, we will select the *initial evolutionary*

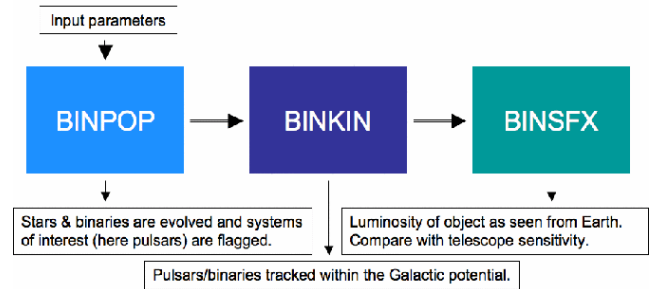


**Figure 2.** Flow chart of our synthetic pulsar population survey process. The work presented here focuses on the first module, BINPOP (see text for details).

parameters from distribution functions and evolve all stars forward in time from stellar birth on the ZAMS through until the current time. This gives us the ability to constrain many stellar and binary evolutionary features while lending us the flexibility to, for example, compare different populations of stars with each other and observations. In this way we can aim to further constrain uncertain parameter values. However, even at this early stage we must place a strong word of caution regarding the issue of parameter variation – strong degeneracies can apply amongst parameters (e.g. O’Shaughnessy et al. 2005), where a succession of parameter changes can mask the effect of another, so extensive modelling is required before definite conclusions can be made.

Our goal is to create a generic code for producing synthetic Galactic populations. This will comprise three modules: BINPOP, BINKIN and BINSFX (see the flow chart in Figure 2 for a representation of how these fit together). The first module, BINPOP, covers the stellar and binary evolution aspects and as such is a traditional population synthesis code in its own right. The second module, BINKIN, follows the positions of both binary systems and single stars within the Galactic gravitational potential. The third module imposes selection effects on the simulations, thus giving simulated data that can compare directly to observations. This last consideration is in some regards the most important as without detailed modelling of selection effects any comparison of population synthesis simulations to observations is crude (Kalogera & Webbink 1998). This paper focuses on a description of the BINPOP module and, in particular, the pulsar population that it produces. We consider in depth modelling of pulsar evolution in terms of the spin period and the magnetic field coupled with mass accretion. Simulating these processes will help in constraining the stellar birth properties of NSs and also lead to a greater understanding of aspects of NS evolution such as the formation event itself – the supernova. It will also allow predictions of the composition of the Galactic pulsar population. Follow-up work will discuss BINKIN with a focus on the kinematic evolution of the pulsar distribution within the Galaxy, and SN velocity kicks – and BINSFX.

This paper is organised as follows. Section 2 gives an overview of the rapid binary evolution population synthesis code used in this research. This is followed in Section 3 by a detailed description of the pulsar modelling techniques that have been added to this code to create BINPOP. Section 4 gives examples of the pulsar evolutionary pathways that can be followed with BINPOP and how these can be affected by

choices in the algorithm. Population synthesis results in the form of  $P\dot{P}$  comparisons are given in Section 5 followed by a discussion in Section 6. In particular we wish to draw the readers attention to the results shown in Section 5.8.5 which extend beyond the basic  $P\dot{P}$  description.

## 2 RAPID BINARY EVOLUTION & POPULATION SYNTHESIS

The research presented here makes use of the first module of our synthetic Galactic population code. This is called BINPOP and wraps the Hurley, Tout & Pols (2002: HTP02) BINARY STELLAR EVOLUTION (BSE) code<sup>2</sup> (with updates as described in Section 3) within a population synthesis package.

The BSE algorithm is described in detail by HTP02 and an overview is given in Kiel & Hurley (2006). The aim of BSE is to allow rapid and robust, yet relatively detailed, binary evolution based on the most up-to-date prescriptions/theories for the various physical processes and scenarios that are involved. In its most basic form the BSE algorithm can be thought of as evolving two stars forward in time – according to the SINGLE STAR EVOLUTION (SSE) prescription described in Hurley, Pols & Tout (2000) – while updating the orbital parameters. After each time-step the algorithm checks whether either star has over-flowed its Roche-lobe and depending on the result the system is evolved accordingly, i.e. as a detached, semi-detached, or contact binary. During these phases the total angular momentum of the system is conserved while orbital and spin changes owing to tides, mass/radius variations, magnetic braking and gravitational radiation are modelled.

Within BSE an effort is made to model all relevant stellar and binary evolutionary processes, such as mass transfer and common-envelope (CE) evolution. Invariably this involves making assumptions about how best to deal with elements of the evolution that are uncertain. An example that is relevant to pulsar evolution is the choices made for the nature of the star produced as a result of the coalescence of two stars, where at least one NS is involved. If the merger involves a NS and a non-degenerate star then a Thorne-Żytkow object (TŻO: Thorne & Żytkow 1977) is created. Detailed modelling of these objects must deal with neutrino physics and processes such as hypercritical accretion and currently the final outcome is uncertain (Fryer, Benz & Herant 1996; Podsiadlowski 1996). Possibilities include rapid ejection of the envelope (the non-degenerate star) to leave a single NS that has not accreted any mass or collapse of the merged object to a BH. In BSE the former is currently invoked – an unstable TŻO. On the other hand, the coalescence of a NS with a degenerate companion is assumed to produce a NS with the combined mass of the two stars, unless the companion is a BH in which case the NS is absorbed into the BH. For steady transfer of material onto a NS – in a wind or via Roche-lobe overflow (RLOF) – it is assumed in BSE that the NS can accrete the material up to the Eddington limit (Cameron & Mock 1967). However, there is some uncertainty as to what

extent this limit applies as there may be cases where energy generated in excess of the limit can be removed from the system (e.g. Beloborodov 1998). For this reason the Eddington limit is included as an option in BSE (HTP02). Another area of uncertainty is what happens to a massive oxygen-neon-magnesium WD when it accretes enough material to reach the Chandrasekhar limit – does it explode as a mass-less supernova or form a NS? Currently BSE follows the models of Nomoto & Kondo (1991) which suggest that electron capture on  $\text{Mg}^{24}$  nuclei leads to an accretion-induced collapse (AIC) and a NS remnant (Michel 1987). In the formation of a NS via the AIC method BSE assumes that no velocity kick is imparted onto the NS while some other population synthesis works have assumed a small but non-zero velocity kick for these NSs (Ivanova et al. 2007; Ferrario & Wickramasinghe 2007). These examples illustrate some of the decision making involved with creating a prescription-based evolution algorithm and the interested reader is directed to HTP02 for a full description as well as a list of options included within the BSE code.

Subsequent to HTP02 the following changes have been made to the BSE algorithm:

- an option to calculate supernova remnant masses using the prescription given in Belczynski, Kalogera & Bulik (2002) which accounts for the possibility of the fall-back of material during core-collapse supernovae (this is now the preferred option in BSE);
- an algorithm to compute the stellar envelope structure parameter,  $\lambda$ , (required in CE calculations) from the results of detailed models (Pols, in preparation) – previously this was set to a constant whereas models show that it varies with mass and evolution age (Dewi & Tauris 2001; Podsiadlowski et al. 2003);
- the addition of equations to detect, and account for, the existence of an accretion disk during mass transfer on to a compact object (following Ulrich & Burger 1976); and,
- an option to reduce the strength of winds from helium stars.

These changes are documented in greater detail by Kiel & Hurley (2006). Further additions to the BSE algorithm relating to pulsar evolution will be described in the next section.

There are also a number of areas where the BSE algorithm could be improved in the future. The integration scheme used for the differential equations in BSE (and for the equations introduced here) employs a simple Euler method (Press et al. 1992) with the time-step depending primarily on the nuclear evolution of the stars. It has been suggested that this will lead to inaccurate results for the orbital evolution, in particular when integrating the tidal equations (Belczynski et al. 2008), and an implementation of a higher-order scheme will be a priority for the next revision of the BSE code. It will also be desirable to include a RLOF treatment for *eccentric* binaries and the addition of an option for tidally-enhanced mass-loss from giant stars close to RLOF (along the lines of Bonačić Marinović, Glebbeek & Pols 2008). Another area of uncertainty is the strength of stellar winds from massive stars (Belczynski et al. 2008). This is a feature which can be varied within BSE but we do not utilise it or examine its effect on compact object formation in this work.

Reflecting the variety of processes involved in binary

<sup>2</sup> See also <http://astronomy.swin.edu.au/~jhurley/> and relevant links.

evolution, and the uncertain nature of many of these, there are inevitably a substantial number of free parameters associated with a binary evolution code. Unless otherwise specified we assume the standard choices for the BSE free parameters as listed in Table 3 of HTP02. This includes setting  $\alpha_{\text{CE}} = 3$  for the CE efficiency parameter. In addition we use the variable  $\lambda$  for CE evolution and the remnant mass relation of Belczynski et al. (2002), as described above. We also use  $\mu_{\text{He}} = 0.5$  in the expression for the helium star wind strength (see Kiel & Hurley 2006 for details) and we impose the Eddington limit for accretion onto remnants. Where applicable (Sections 4 and 5) we will take care to note our choices for any BSE parameters that we vary.

Our aim is to produce a Galactic population of pulsars. We do this using the statistical approach of population synthesis. The first step is to produce realistic initial populations of single and binary stars. For each initial binary the primary mass, secondary mass and orbital separation are drawn at random from distributions based on observations (see Section 5.1 for details). For single stars only the stellar mass is required for each star. We then set a random birth age for each binary (or star) and follow the evolution to a set observational time. By selecting those systems that evolve to become pulsars we can produce a  $P$  vs  $\dot{P}$  diagram for the Galactic pulsar population – assuming (at least initially) that all generated pulsars are observable. This is repeated for a variety of models and comparisons made to observations. This is the method we use here. However, it is possible to determine the initial parameters from a set grid and then convolve the results with the above mentioned initial distribution functions to determine if the binary contributes to the Galactic population. For more information on the grid method see Kiel & Hurley (2006).

### 3 MODELLING A PULSAR

We now describe our methods for evolving pulsars – both isolated and within a binary system. This requires a number of additions to the BSE algorithm. We point out here that although most important phases of stellar and binary evolution are modelled we still draw the initial pulsar evolutionary parameters – spin period and magnetic field – from distributions. This is the method employed in all previous pulsar population synthesis simulations. The need for this arises because there is no complete theoretical method for modelling the SN event (Janka et al. 2006), and thus no strong link between the pre-SN star and post-SN star. Aspects such as the initial NS mass, however, are better determined. Also, kick velocities imparted to NSs at birth are generally selected from distributions that match observations of NS space velocities. We investigate the initial NS spin period and magnetic field distributions and extend previous studies by linking these to this kick velocity (see Sections 3.4 and 5.5). We also note that although some previous pulsar population synthesis studies take into account selection effects to allow direct comparison with observations we do not do this here in any detail. As a first step we do consider beaming effects but mainly we leave this for future work. Our wish at this stage is to test that our evolution algorithm can populate the required regions of the observed parameter space. Considering direct number and birth rate comparisons with

observations will follow when the full three module code is complete.

#### 3.1 Previous efforts

There have been many attempts at modelling NS evolution. Some, as given in the introduction, try to generalise or parametrise the evolution to allow rapid computation for statistical considerations. Another method, however, is to perform detailed modelling of a single NS. Debate on NS evolution has concentrated mainly on the structure of NSs and the evolution of the magnetic field. Most statistical studies have considered only those NSs that are isolated pulsars and here concern is, generally, on the magnetic field decay timescale or space velocity and magnetic field correlation. The semi-analytical studies of Gunn & Ostriker (1970), Phinney & Blandford (1981), Vivekanand & Narayan (1981) and Lyne, Manchester & Taylor (1985) found a magnetic field decay timescale of order a few million years. In comparison, studies by Taylor & Manchester (1977), van den Heuvel (1984) and Stollman (1987) found the decay timescale to be  $> 100$  Myr. More recently population studies of pulsars have tended towards a greater level of detail in the treatment of pulsar evolution and modelling of selection effects. Again, differing studies find a variation of magnetic field decay time-scales. Those such as Bailes (1989), Rathnasree (1993); Bhattacharya et al. (1992), Hartman et al. (1997), Lorimer et al. (1993), Lorimer, Bailes & Harrison (1997), Regimbau & de Freitas Pacheco (2000), Regimbau & de Freitas Pacheco (2001), Dewi, Podsiadlowski & Pols (2005) and Faucher-Giguere & Kaspi (2006) conclude that field decay occurs on timescales comparable to the age of old pulsars. While Gonthier et al. (2002) and Gonthier, Van Guilder & Harding (2004) suggest NSs evolve with shorter decay time-scales ( $\sim$  few Myr). However, Faucher-Giguere & Kaspi (2006) suggest this later result is an artifact of the pulsar radio luminosity law assumed by Gonthier et al. (2002) and Gonthier, Van Guilder & Harding (2004). The field decay time-scale is a parameter within our models that is allowed to vary. As we will here, Dewey & Cordes (1987), Bailes (1989), Rathnasree (1993), Dewi, Podsiadlowski & Pols (2005) and Dai, Liu & Li (2006) take into consideration pulsars that may evolve within binary systems and follow the orbital properties along with the pulsar spin and magnetic field. Previously either the treatment of binary evolution or pulsar evolution has been limited, although the work of Dai, Liu & Li (2006) utilises the BSE and a limited form of pulsar physics. No published work to date has fully considered the effect of magnetic field decay within both single and binary pulsar evolution in such detail as presented here.

#### 3.2 Single or wide binary pulsar evolution

We first consider the evolution of a NS that does not accrete any material, either an isolated NS or one in a wide enough orbit to allow single star-like evolution. Although, in the latter case we note that aspects of binary evolution such as tidal interaction are followed in step with the pulsar spin evolution. We evolve a solitary pulsar by assuming a pulsar magnetic-braking model of the form,

$$\dot{P} = K \frac{B_s^2}{P}, \quad (1)$$

(Ostriker & Gunn 1969) with  $\dot{P}$  [s/s],  $B_s$  [G],  $P$  [s] and  $K \sim 6.3 \times 10^{-54}$  [ $R_\odot^3 s M_\odot^{-1}$ ]. Here it is assumed that the beam is  $90^\circ$  to the pulsar equator. This is of course a simplification because the beam must be off-axis to pulse (Spitkovsky 2006). Other methods of pulsar spin evolution may be included in future iterations of the model. Some more examples are magnetar spin-down evolution (Harding, Contopoulos & Kazanaz 1999) and spin-down of oblique (Contopoulos & Spitkovsky, 2006; Spitkovsky 2006) or perpendicular rotators (Goldreich & Julian 1969). The magnetic field is also assumed to evolve in time due to ohmic dipole decay which, in its simplest form, may be modelled as,

$$B_s = B_{s0} \exp\left(-\frac{T - t_{\text{acc}}}{\tau_B}\right), \quad (2)$$

where  $B_{s0}$  is the initial NS surface magnetic field,  $T$  is the age of the pulsar,  $\tau_B$  is the magnetic field decay time-scale and  $t_{\text{acc}}$  is the time the pulsar has spent accreting matter via RLOF. Allowing the magnetic field to decay is inspired by observations, where older isolated pulsars are shown to have lower magnetic fields than younger pulsars and is now a standard evolutionary model within the literature (Gunn & Ostriker 1969; Stollmen 1987). This apparent magnetic field decay is still observed even when detailed modelling of selection effects are taken into account (Faucher-Giguere & Kaspi 2006), though as mentioned above the timescale varies due to assumptions used within the modelling. To integrate these equations into the BSE we must follow the angular momentum of the NS using the magnetic-braking model of Equation 1. Differentiating the angular velocity with time and applying the chain rule we have the angular velocity time derivative,

$$\dot{\Omega} = -\frac{\Omega}{P} \dot{P} \quad (3)$$

Substituting Equation 1 into Equation 3 allows us to find the angular velocity rate of change (here it is a spin-down effect) in terms of the intrinsic features of the pulsar,

$$\dot{\Omega} = -K \frac{\Omega}{P^2} B_s^2 \quad (4)$$

$$= -\frac{K}{4\pi^2} \Omega^3 B_s^2 \quad (5)$$

$$= -K_2 \Omega^3 B_s^2 \quad (6)$$

where  $K_2 \sim 2.5 \times 10^{-52}$ . It is Equation 6 which we use directly with the code, evolving the NS magnetic-braking angular momentum,  $J_{\text{mb}}$  with,

$$\dot{J}_{\text{mb}} = \frac{2}{5} M R^2 \dot{\Omega}, \quad (7)$$

which is the angular momentum equation for a solid spherical rotator with radius  $R$ , mass  $M$  and angular velocity  $\Omega$ . This is then removed from the total NS angular momentum, the system is updated (this includes the NS spin-down being transferred to the orbital angular momentum via tides) and we step forward in time.

In the work presented here we are evolving the surface magnetic field,  $B_s$  of the NS. Strictly speaking if we were to compare our theoretically calculated magnetic field to observations we should use the magnetic field strength at the

light cylinder radius – that is the radius at which if the magnetic field is considered a solid rotator it is rotating at the speed of light. When observations of the spin period and spin period derivative are made it is the magnetic field at this radius that is being sampled. When we calculate the period derivative this assumed change of magnetic field is taken into account and as such we have two reasons for comparing our theoretical models to observations in the period-period derivative parameter space. Firstly, it is  $\dot{P}$  that is actually being measured observationally and secondly the  $\dot{P}$  calculation naturally takes into account the light cylinder magnetic field (as it makes use of the pulsar magnetic moment).

### 3.3 Pulsar evolution during accretion

Allowing the decay of a NSs magnetic field during an accretion event is believed to be the cause of the observed pulsar  $P\dot{P}$  distribution (see Section 1). Until now this has not been tested with any detailed modelling of binary, stellar and pulsar evolutionary physics. During any accretion phase angular momentum is transferred to the accreting object and it is spun-up. To follow this evolution we use the standard equations describing the system angular momentum as given in HTP02. While steady mass transfer occurs we do not allow any decrease in the NS rotational velocity due to the magnetic-braking process described by Equation 6. Instead the NS angular momentum increases while the magnetic field decays exponentially with the amount of mass accreted,

$$B_s = B_{s0} \exp\left(-k \frac{\Delta M}{M_\odot}\right), \quad (8)$$

where  $k$  is a scaling parameter that determines the rate of decay. Although there is no physical basis for Equation 8 if accretion onto a NS does cause – even at the very least – an apparent decay of the NS magnetic field then the process must be tied, in some manner, to the accreted mass (see Section 1). A similar method of magnetic field evolution during accretion was first suggested by Shibazaki et al. (1989) and Romani (1990), with their equation of,

$$B_s = \frac{B_{s0}}{1 + \frac{\Delta M}{M_\star}}, \quad (9)$$

which is comparable to our Equation 8.  $M_\star$  is a parameter that Shibazaki et al. (1989) fit to observations and found to be of order  $10^{-4} M_\odot$ . Similar to Shibazaki et al. (1989) we do not assume any particular model of field decay during the accretion phase (i.e. burial of field lines, see Section 1), only that field decay following Equation 8 does occur.

Typical accretion onto a NS has the in-falling matter interacting with the magnetosphere. Once the magnetic pressure dominates the gas pressure the matter is channelled along magnetic field lines to be accreted onto the magnetic poles (Pringle & Rees 1972). Not all mass transfer events within a binary system, however, result in accretion of material. One such example with much relevance here is the ‘propeller’ (Illarionov & Sunyaev 1975) phase (Davidson & Ostriker 1973; Illarionov & Sunyaev 1975; Kundt 1976; Savonije & van den Heuvel 1977). Here we have a NS with a sufficiently large magnetic field and rotational velocity. The mass being transferred from the companion falls towards



the NS but instead of following the magnetic field lines to the surface the material is ejected from the system by the rapidly rotating magnetic field lines. The magnetic field acts as a propeller, changing rotational energy of the NS into kinetic energy for the now outgoing matter. This phase has a noticeable effect on the NS. Due to the loss of rotational energy by the NS it spins down. This is therefore an important evolutionary phase to consider during accretion and we have implemented a method for modelling it within BSE. We follow Jahan-Miri & Bhattacharya (1994) who allow the difference between the Keplerian angular velocity,  $\Omega_K$ , at the pulsar magnetic radius  $R_M$  and the co-rotation angular velocity,  $\Omega_*$ , ( $V_{\text{diff}} = \Omega_K(R_M) - \Omega_*$ ) to decide whether the accretion phase spins the NS up or down. The magnetic radius is assumed to be half the Alfvén radius,  $R_m$ , the radius at which the magnetic pressure balances the ram-pressure,

$$\frac{B_s^2 R^6}{8\pi R_m^6} = \frac{(2GM)\dot{M}}{4\pi R_m^{5/2}}. \quad (10)$$

This gives

$$R_m = 3.4 \times 10^{-4} R_\odot \left( \frac{B_s^2 R^6}{M^{1/2} \dot{M}} \right)^{2/7}. \quad (11)$$

The rate of change of the angular momentum for an accreting NS is then (cf. Equation 2 Jahan-Miri & Bhattacharya 1994),

$$\dot{J}_{\text{acc}} = \epsilon V_{\text{diff}} R_M \dot{M}, \quad (12)$$

where  $\epsilon$  is a parameter that allows for any uncertainties in the efficiency of coupling the magnetic field and matter. During wind accretion  $\epsilon$  is considered unity, however, when Roche-lobe mass transfer occurs we allow  $\epsilon$  to vary slightly with the mass transfer rate, that is  $\epsilon \sim 10^{-14}/\dot{M}$  (see Jahan-Miri & Bhattacharya 1994). Jahan-Miri & Bhattacharya (1994) conclude that this method is relatively robust given much of the physics of accretion and capture flow are ignored. A similar though slightly more detailed method is used within the pulsar population synthesis work of Possenti et al. (1998). During the propeller phase we assume that the entire discarded matter leaves the binary system.

Something that has not received a large amount of attention in binary NS population synthesis work is the assumed amount of angular momentum gained by a NS when accreting mass via a wind from its companion (see however the informative works of Liu & Li 2006; Dai, Liu & Li 2006). Because the spin histories of NSs are important for our comparisons to observations, angular momentum accretion is something that we feel should be examined. In particular this evolutionary phase may be important when modelling the apparent bridge of observed pulsars that connect the standard pulsar island to the recycled island. To examine this effect we multiply the angular momentum of the accreted mass by the efficiency parameter  $\Xi_{\text{wind}}$  giving,

$$\Delta J_{\text{wind}} = \frac{2}{3} \Xi_{\text{wind}} \Delta M R_2^2 \Omega_2, \quad (13)$$

where  $J_{\text{wind}}$  is the angular momentum transferred in the wind,  $\Delta M$  is the accreted mass,  $R_2$  is the companion stellar radius and  $\Omega_2$  is the companion star angular velocity. Basing the variability of  $\Xi_{\text{wind}}$  on the assumption that the NS magnetic field plays an integral part when NS angular momentum accretion occurs, we allow  $\Xi_{\text{wind}}$  to vary as,

$$\Xi_{\text{wind}} = \text{MIN} \left( 1, 0.01 \left( 2 \times 10^{11} / B_s \right) + 0.01 \right). \quad (14)$$

By assuming the above form of  $\Xi_{\text{wind}}$  we allow larger magnetic fields to dominate the flow of angular momentum, while the simplicity depicts our lack of knowledge of the physical processes in such an evolutionary phase. An example of the uncertainty is shown in the work of Ruffert (1999) who estimates an angular momentum accretion efficiency between 0.01 and 0.7 (hence our lower limit for  $\Xi_{\text{wind}}$ ).

### 3.4 Initial pulsar parameter selection

As mentioned earlier previous pulsar population synthesis work begin by selecting the initial period, magnetic field, mass, etc, of the pulsar from distributions, ignoring any earlier evolutionary stages the star may have passed through. If the distributions for each parameter are realistic this method is considered robust to first order. This is the method followed here for the initial spin period of the pulsar,  $P_0$ , and the initial surface magnetic field,  $B_{s0}$ . We select from flat distributions between  $P_{0\text{min}}$  and  $P_{0\text{max}}$  for the initial spin period and between  $B_{s0\text{min}}$  and  $B_{s0\text{max}}$  for the initial magnetic field. Typical values for these parameters are  $P_{0\text{min}} = 0.01$  s,  $P_{0\text{max}} = 0.1$  s,  $B_{s0\text{min}} = 10^{12}$  G and  $B_{s0\text{max}} = 3 \times 10^{13}$  G, although these can vary (see Table 1).

In actual fact the exact initial pulsar spin period and magnetic field distributions are unknown. However, Spruit & Phinney (1998) have previously suggested that there is a connection between the three pulsar birth characteristics: imparted velocity, spin period and magnetic field strength. A parameter linked to the SN event and one in which we claim to have some form of observational constraint is  $\mathbf{V}_{\text{kick}}$ . The velocity kick is randomly selected from a Maxwellian distribution with a dispersion of  $V_\sigma$  (as in HTP02 and Kiel & Hurley 2006). With this in mind we trial a method in which the initial pulsar birth parameters  $P_0$  and  $B_{s0}$  are linked to  $\mathbf{V}_{\text{kick}}$ . In this ‘SN-link’ method we have,

$$P_0 = P_{0\text{min}} + P_{0\text{av}} (V_{\text{kick}}/V_\sigma)^{n_p}, \quad (15)$$

and

$$B_{s0} = B_{s0\text{min}} + B_{s0\text{av}} (V_{\text{kick}}/V_\sigma)^{n_b}, \quad (16)$$

where  $P_{0\text{av}}$  is the average initial period and  $B_{s0\text{av}}$  is the average initial magnetic field. The exponents  $n_p$  and  $n_b$  allow us to parameterise the effect the SN event has on the initial pulsar period and magnetic field but we take both equal to one throughout this work. An assumption here is that a more energetic explosion would be able to impart a greater initial angular velocity onto the proto-NS than a lesser explosion, which may in turn introduce a more effective dynamo action increasing the initial magnetic field strength.

We note here that due to the lack of a complete understanding of SNe, we are at present not attempting to find the true pulsar initial period and magnetic field distributions *but* trying to depict how modifying the initial pulsar birth region in the  $P\dot{P}$  distribution affects the final pulsar  $P\dot{P}$  distribution. Previous population synthesis models have differed on their preferred initial parameter distributions (compare Faucher-Giguere & Kaspi 2006 and Gonthier, Van Guilder & Harding 2004; Story, Gonthier & Harding 2007), however, any complete pulsar population synthesis must be able to reproduce the observed pulsars associated with SN remnants.

### 3.5 Electron capture supernova

An important phase in NS evolution which we have touched on briefly already is the birth of NSs in SN events. Previous numerical models of SNe suggested that convection may drive the formation of asymmetries in SNe (Herant, Benz & Colgate 1992; Herant et al. 1994). More recently there have been exciting developments in this area driven by the successful modelling of SN explosions in multi-dimensional (spatially) hydrodynamic simulations (Mezzacappa et al. 2007; Marek & Janka 2007; Fryer & Young 2007). These models show high levels of convection due to the stationary accretion shock instability (found numerically by Blondin & Mezzacappa 2003). This instability leads to an asymmetry in the explosion event and provides a mechanism for delivering large SN velocity kicks. Observationally, proper motion studies of pulsars have detected large isolated pulsar space velocities of order 1000 km/s (e.g. Lyne & Lorimer 1994). Furthermore, mean pulsar space velocities appear to be in excess of the mean for normal field stars (e.g. Hobbs et al. 2005). These results show the necessity of imparting velocity kicks to NSs. As such most previous population synthesis works have assumed a Maxwellian SN velocity kick distribution with  $V_\sigma \sim 200 - 500$  km/s (see above in Section 3.4).

Of late however, there has been a body of evidence that some NSs must have received small velocity kicks, of order 50 km/s (Pfahl et al. 2002; Podsiadlowski et al. 2004). Observationally Pfahl et al. (2002) found a new type of high-mass X-ray binary which exhibited low eccentricities and wide orbits, suggesting a low velocity kick imparted during the SN event. This is backed up by evidence of the relatively large amount of NSs within globular clusters compared to the estimated number if one considers they receive an average velocity kick of  $V_\sigma > 200$  km/s (Pfahl, Rappaport & Podsiadlowski 2002; and more recently in the theoretical studies of Kuranov & Postnov 2006 and Ivanova et al. 2007). The type of SN explosion that theoretically causes small velocity kicks, and is in vogue at present, is the electron capture (EC) method. Basically this is the capture of electrons in the stellar core by the nuclei  $^{24}\text{Mg}$ ,  $^{24}\text{Na}$  and  $^{20}\text{Ne}$  (Miyaji et al. 1980, see their Figure 8 and Table 1). This results in a depletion of electron pressure in the core, facilitating the core collapse to nuclear densities if the final core mass is within the mass range of 1.4 to 2.5  $M_\odot$  (Nomoto 1984; 1987). The bounce of material due to the halt of the collapse by the strong force thus drives the traditional SN event. Taking into account both single star evolution (Poe-larends et al. 2007) and binary evolution (Podsiadlowski et al. 2004) suggests that the initial mass range of stars that may explode via the EC SN mechanism resides somewhere within 6 – 12  $M_\odot$ , with some dependence on metallicity and assumptions made in stellar modelling. Early work on the EC SN explosions suggested that it is a prompt event, in which any asymmetries would not have time to occur. Thus allowing the nascent NS a small SN kick velocity. This is in contrast to SN explosions from more massive initial mass stars ( $> 12 M_\odot$ ) which produce rather slow explosions (many hundreds of ms; Marek & Janka 2007). We note that the latest oxygen-neon-magnesium SN explosions (initial stellar mass range of 8 – 12  $M_\odot$ ) by Kitaura, Janka & Hillebrandt (2006) show that the EC SN is not so prompt as previously thought (few hundred ms) and also energy yields

are a factor of 10 less. However, these authors still find low recoil velocities for the nascent NS, again because hydrodynamic instabilities are unlikely to form.

As detailed in Ivanova et al. (2007) there are a number of stellar and binary evolutionary pathways which may lead to EC SN. Although EC SN may occur from processes of single star evolution we concentrate here on a relatively newly recognised binary evolution example (Podsiadlowski et al. 2004). A primary star with a zero-age-MS mass between  $\sim 8 - 12 M_\odot$  that lives in the appropriate binary system may experience a mass transfer phase in which its convective envelope is stripped from it before the second dredge-up phase on the asymptotic giant branch. This lack of second dredge-up leaves behind a more massive helium core than would otherwise have remained if the hydrogen-rich envelope had not been stripped off. Yet it is a less massive core than is left behind for stars  $> 12 M_\odot$  (see Podsiadlowski et al. 2004, Figure 1). Depending upon the rate of mass loss via a wind the helium core may then evolve through the relevant phases to explode as an EC SN (Podsiadlowski et al. 2004). The ability for a binary system to produce a helium star with a mass within the assumed range of 1.4 to 2.5  $M_\odot$  as given above is much greater than for a single star (Podsiadlowski et al. 2004).

The possibility of EC SNe is included as an option in BSE for the following cases:

- a giant star with a degenerate oxygen-neon-magnesium core that reaches the Chandrasekhar mass – for the stellar evolution models used in BSE this corresponds to an initial mass range of  $\sim 6 - 8 M_\odot$  (for solar metallicity: HTP02);
- a helium star with a mass between 1.4  $M_\odot - 2.5 M_\odot$  (as set by Podsiadlowski et al. 2004 based on the work of Nomoto 1984; 1987).

When a NS forms in these cases we use an electron capture kick distribution with  $V_\sigma = 20$  km/s (see NS kick distribution of Kiel & Hurley 2006).

### 3.6 NS magnetic field lower limit

Most detailed magnetic field decay models show a ‘bottom’ or lower limit value of the magnetic field in which no further decay is possible. Here, this lower limit is a model parameter,  $B_{\text{bot}}$ , and, as given in Zhang & Kojima (2006), should be of order  $10^7 - 10^8$  G. We use  $5 \times 10^7$  G throughout this work.

### 3.7 Radio emission loss: The death line

Generally, it is believed electron-positron pairs are the particles that, when accelerated within the magnetic field of a NS, produce the observed radio emission. These pairs are assumed to form in the polar cap (PC) region of the NS (PC model: Arons & Scharlemann 1979; Harding & Muslimov 1998) or in the outer NS magnetosphere beyond the polar caps (as in the outer gap model: Chen & Ruderman 1993). Depending upon the chosen model it is possible to predict when or under what circumstances a NS will turn off its beam mechanism and thus stop being observable as a pulsar. These predictions form a region in the  $P\dot{P}$  parameter space where the NS is not able to sustain pair production. The edge of this region is commonly referred to as the pulsar death line. Until recently efforts within pulsar population



synthesis calculations for simulating the death-line have only considered isolated pulsars. Such models have been based on the work by Bhattacharya et al. (1992) who, following Ruderman & Sutherland (1975), give the condition,

$$\frac{B_s}{P^2} > 0.17 \times 10^{12} G/s^2. \quad (17)$$

Zhang, Harding & Muslimov (2000) extend the above equation to consider differing forms of particle scattering and acceleration methods but still only consider isolated pulsar evolution when constructing their pulsar death line models. These conditions, however, do not consider the physics involved in rapidly rotating NSs, such as MSPs, and can not account for the observed pulsar cut off at lower periods.

Here we must turn to the work of Harding, Muslimov & Zhang (2002, henceforth HMZ) who, when considering the PC model, make allowance for MSP spin periods and masses. In the long line of work completed in this field (Harding & Muslimov 1998, 2001, 2002; HMZ) it is shown that there are a number of conditions which can be used to differentiate between the pair-production domain and the pair-production prohibited domain. These conditions rely heavily on two factors, (1) the type of radiation that forms a cascade of the aforementioned pair-produced particles and (2) the height at which this cascade develops – the pair formation front. For (1) HMZ calculate models based on three radiation dominant pair-production mechanisms. They assume the pair-produced particles may be created by curvature radiation (CR), which itself is released from accelerated particles forced to move along curved magnetic field lines, or via inverse Compton scattering (Hibschman & Arons 2001; HMZ), that is, soft photons (i.e. relatively low energy photons) being scattered to high energies by accelerated high energy charged particles. If a small number of these soft photons have energies near the cyclotron frequency they will scatter with a much greater cross section and thus provide a larger number of high energy photons (the inverse Compton photons). Therefore, HMZ consider two inverse Compton models, resonant inverse Compton scattering and nonresonant inverse Compton scattering. For (2), if the pair formation front occurs at an altitude less than the radius of the polar cap (defined by the strength of the magnetic field) the pulsar is said to be unsaturated. If the pair formation front is at an altitude greater than the polar cap radius the pulsar is in the saturated regime. These regimes are important because they determine in what type of electric field the pair-produced particles are accelerated in. Unsaturated pairs may accelerate in an increasing (in altitude) electric field (parallel to the magnetic field lines), while saturated pairs are accelerated in a constant electric field.

In this work, for simplicity, we limit ourselves to only consider the CR death line HMZ model. Our slightly modified HMZ-CR death line equations are:

$$P < P_*^{\text{CR}}, \quad (18)$$

$$\log(\dot{P}) = \frac{21}{8} \log(P) - \frac{7}{4} \log(\bar{f}_{\text{prim}}^{\text{min}}) \quad (19)$$

$$-\frac{3}{2} \log(I) + \frac{19}{2} \log(R) - 9.66 \quad (20)$$

$$P > P_*^{\text{CR}} \quad (21)$$

$$\log(\dot{P}) = \frac{5}{2} \log(P) - 2 \log(\bar{f}_{\text{prim}}^{\text{min}}) \quad (22)$$

$$-\frac{3}{2} \log(I) + 11 \log(R) - 19.84, \quad (23)$$

where,  $P < P_*^{\text{CR}}$  is the unsaturated regime and  $P_*^{\text{CR}} = 4.64 \times 10^{-7} B_s^{4/9}$  is the CR saturated-unsaturated limit in seconds. The modification simply allows the use of solar units for  $M$  and  $R - B$  is in Gauss,  $P$  in seconds. A strength of the HMZ death lines is the fact that stellar evolutionary features such as mass and radius play a role in how the radio emission is formed. In fact, HMZ show how important binary mass transfer is in modifying the death line equations. Thus one parameter included within these equations is the NS moment of inertia,  $I$ , which we wish to calculate. To calculate  $I$  we are required to assume an equation of state and mass-radius relationship,

$$I = \frac{2}{7} \left( 1 - 2.42 \times 10^{-6} \frac{M}{R} - 2.9 \times 10^{-12} \frac{M^2}{R^2} \right)^{-1} MR^2 \quad (24)$$

and

$$R = 2.126 \times 10^{-5} M^{-1/3}. \quad (25)$$

Here,  $I$  is taken from Tolman (1939) and as shown in Figure 6 of Lattimer & Prakash (2001) this equation is a good fit to detailed models of NSs for differing equation of states down to  $\frac{M}{R} \sim 10^{-7} M_{\odot}/R_{\odot}$ . HMZ show that the pulsar death line is particularly sensitive to the assumed equation of state, any future work on this area must take this into consideration. After assuming an equation of state and mass-radius relation we may still modify the effect of the HMZ death-line equations by varying  $\bar{f}_{\text{prim}}^{\text{min}}$ , the minimum pulsar efficiency required for pair production to occur, a parameter used by HMZ to fit their parameterised equations to detailed model results. Harding & Muslimov (2002) suggest upper and lower bounds on what value  $\bar{f}_{\text{prim}}^{\text{min}}$  should take for each model. For CR these values are 0.1 and 0.5 for lower and higher respectively.

## 4 SOME EVOLUTION EXAMPLES

To examine the newly implemented BSE pulsar evolution we now take a detailed look into the evolution of an isolated pulsar and a binary system containing a pulsar. This also allows us to investigate how sensitive pulsar evolution is to uncertain parameters in the binary and pulsar model.

### 4.1 An isolated pulsar

We begin by considering an isolated  $20 M_{\odot}$  star initially residing on the main-sequence (MS) with solar metallicity,  $Z = 0.02$ . This star very quickly becomes a  $2.3 M_{\odot}$  NS; spending only 8.8 Myr as a MS star, 0.016 Myr on the Hertzsprung gap (HG), skipping the first giant branch to ignite core helium burning (which lasts for 1.0 Myr) and then moving onto the first asymptotic giant branch, where after 0.02 Myr it becomes a NS. The NS, when born, is given a randomly selected spin period of  $P_0 = 2 \times 10^{-2}$  s and a surface magnetic field of  $B_{s0} = 5.0 \times 10^{12}$  G. This means the NS in this example has a period derivative of  $\dot{P}_0 = 8.5 \times 10^{-12}$  s/s. The subsequent evolution of the NS

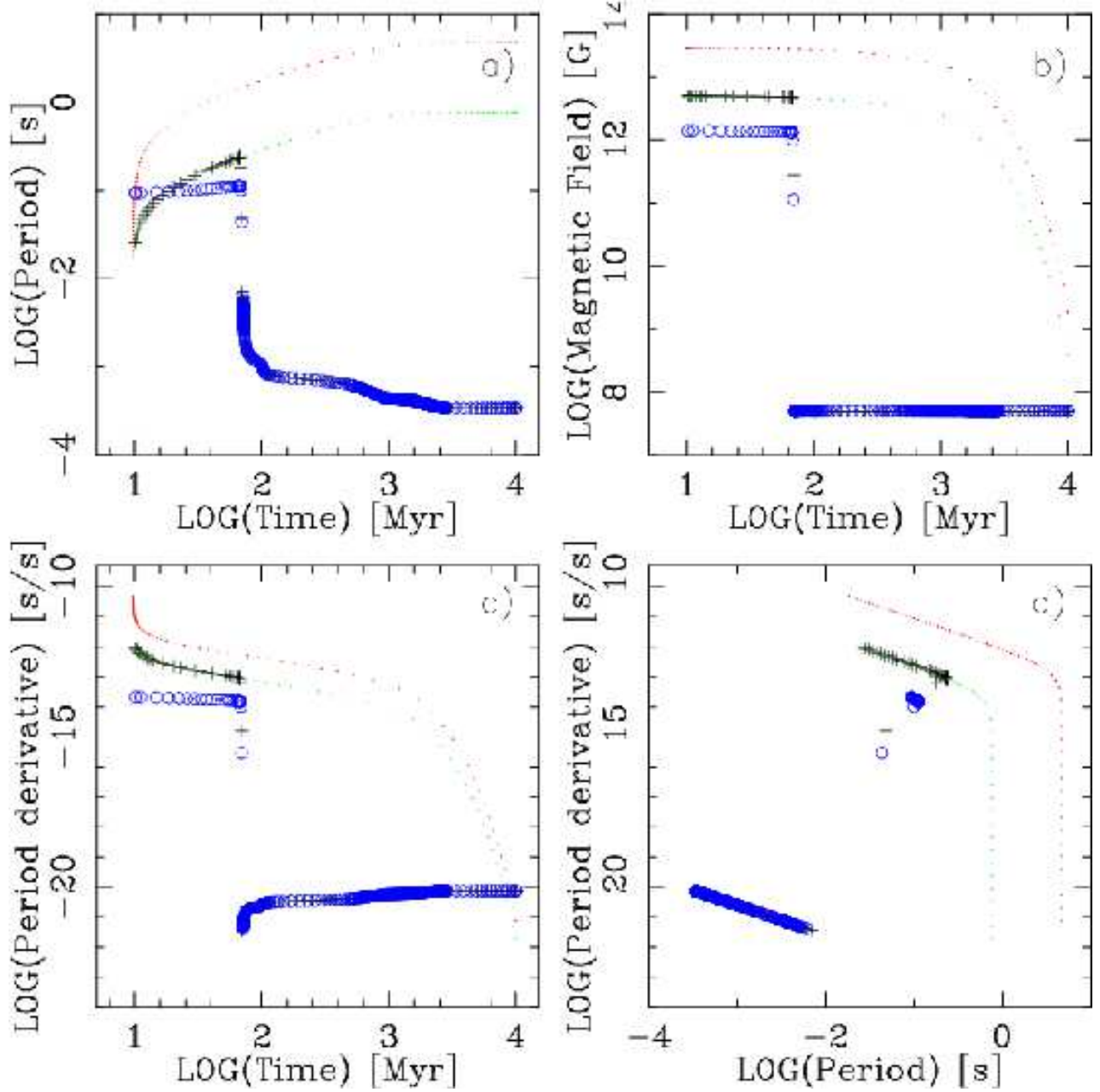


**Figure 3.** The evolution of pulsar particulars,  $P$ ,  $B_s$  and  $\dot{P}$  for differing initial parameter  $P$  and  $B_s$  values. There are two isolated pulsar evolutionary pathways depicted here, these are the dotted paths. Two binary pulsar evolutionary paths are also shown (pluses and circles). See text for further details.

spin period, magnetic field and period derivative are shown in Figures 3a), b) and c) respectively (the lower dotted curves in each plot). The evolution in the  $P\dot{P}$  diagram is shown in Figure 3d).

After 10 Gyr the stellar spin period, magnetic field and period derivative are ‘observed’ as,  $0.76$  s,  $3.7 \times 10^8$  G and  $2.04 \times 10^{-22}$  s/s respectively. No pulsar has ever been observed with such parameters, so it is safe to assume that this NS, after 10 Gyr, would be beyond the pulsar death line. In fact, if we assume a death line of the form given by Equation 17 then the pulsar would die after a system time of 4555 Myr. This is the case if we assume  $\tau_B = 1000$  Myr. However, if we assume instead that the magnetic field

decays on a much faster time-scale, say,  $\tau_B = 5$  Myr, then the NS parameters evolve to a somewhat different configuration. In this case the NS ends with  $P = 6.9 \times 10^{-2}$  s,  $B_s = 5 \times 10^7$  G and  $\dot{P} = 3.6 \times 10^{-23}$  s/s. Here the NS magnetic field reaches the lower limit of  $5 \times 10^7$  G in just over 600 Myr which is about the same time that the pulsar would cross the death line. If we assume the star has a metallicity of 0.001 or 0.0001 then a BH is born directly. This is because the boundary between NS and BH formation (which is governed by the asymptotic giant branch core mass which collapses to a  $3 M_\odot$  remnant) varies slightly with metallicity. In terms of initial stellar mass this is about  $21 M_\odot$  for

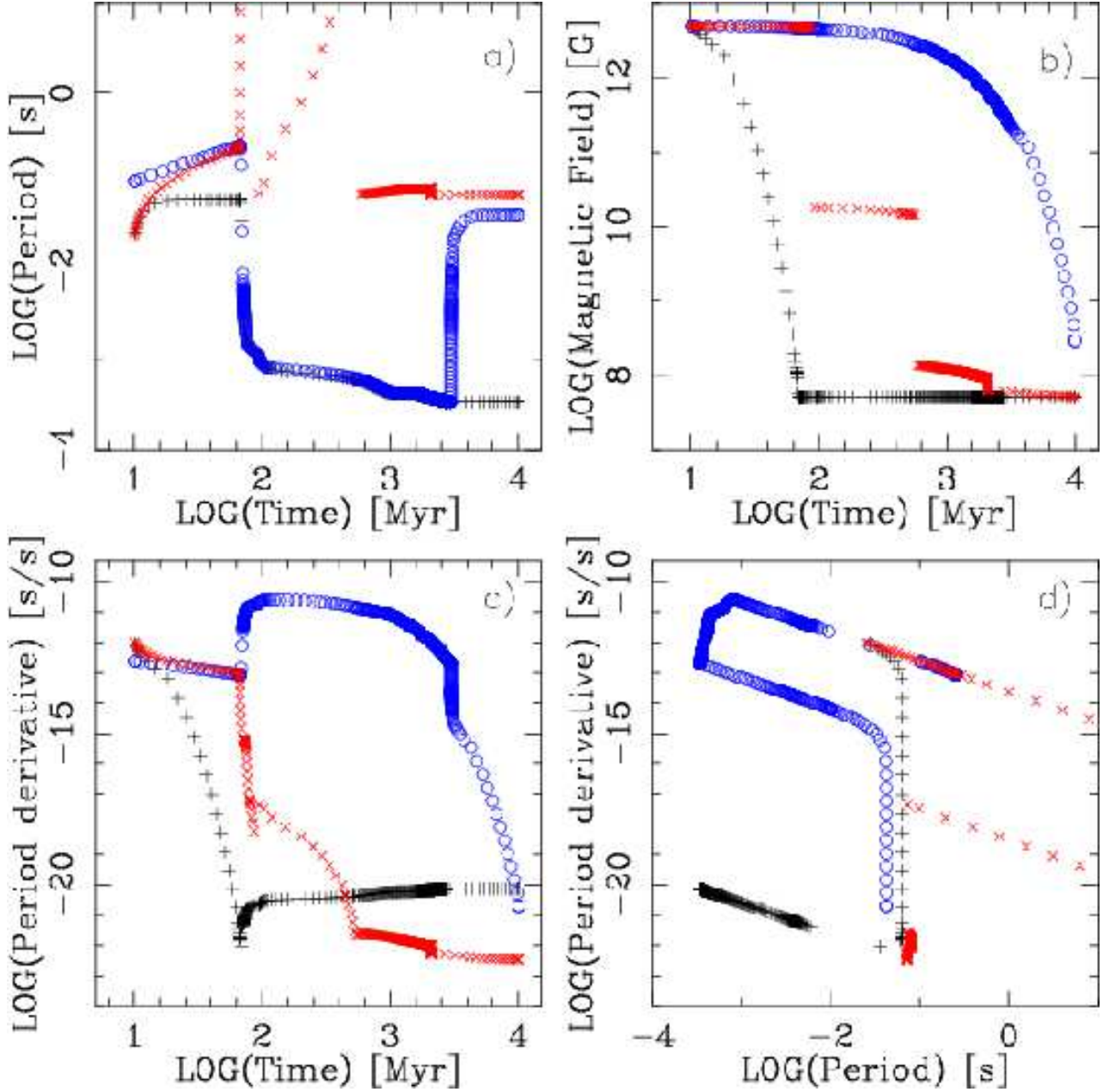


**Figure 4.** The evolution of pulsar particulars,  $P$ ,  $B_s$  and  $\dot{P}$  for differing evolutionary assumptions,  $\tau_B$  (plus),  $k$  (circles) and *propeller* (cross).

solar metallicity whereas for a  $Z = 0.0001$  population it is  $19 M_\odot$ .

#### 4.2 A binary MSP

We now consider the same NS/pulsar as before but place it within a binary system. The initially  $20 M_\odot$  primary star (NS progenitor) has a  $5.5 M_\odot$  companion in a circular  $P_{\text{orb}} = 32$  day ( $a = 125 R_\odot$ ) orbit. Initially the stars are assumed to reside on the ZAMS. Due to the greater mass of the primary star it evolves more quickly than its secondary companion, leaving the MS at the same time as its isolated counterpart of the previous example (as compared to the secondary, who leaves the MS after 540 Myr). The primary

evolved to fill its Roche-lobe at a system time of 8.8 Myr. At this point it is in the HG phase of evolution and has lost  $\sim 1 M_\odot$  in a stellar wind – the secondary accreted  $0.285 M_\odot$  of this and was spun up accordingly. At the onset of RLOF mass transfer occurred on a dynamical timescale and lead to formation of a common-envelope. During the common envelope phase the MS secondary and the primary core spiral in toward each other with frictional heating expelling the CE. This phase is halted when the entire envelope is removed ( $\sim 14 M_\odot$ ) and the two stars are just  $8 R_\odot$  apart. At this stage the MS secondary star is extremely close to overflowing its Roche-lobe radius, however, the primary star – now being a naked helium star – continues to release mass in the form of a wind (which we assume has the form given in

Kiel & Hurley 2006) and due to conservation of angular momentum begins to increase the distance between the stars. The secondary star accretes a small fraction of this wind material and grows to a mass of  $5.815 M_{\odot}$ . Then, after just 10 Myr the primary star goes SN ejecting a further  $3 M_{\odot}$  instantly from the system to become a  $1.7 M_{\odot}$  NS. An eccentricity of 0.4 is induced into the orbit and the separation is now increased to  $15 R_{\odot}$ . By the time the secondary star evolves enough to initiate steady mass transfer, at a system time of 67 Myr, the orbit has been circularised by tidal forces acting on the secondary stars' envelope. The accretion phase lasts for 2800 Myr. Within this time the secondary star evolves from the MS to the HG and then onto the first giant branch. During accretion the secondary loses  $5.6 M_{\odot}$ , the NS accretes  $1.1 M_{\odot}$  and the separation increases out to  $32 R_{\odot}$ . Beyond this the system does not change greatly. After a short time ( $\sim 30$  Myr) the secondary evolves to become a  $0.2 M_{\odot}$  helium WD (HeWD) – being stripped of its envelope the WD does not develop any deep mixing to form a higher metallicity content in its envelope (e.g. such as carbon-oxygen or oxygen-neon-magnesium WDs). At the end of the simulation we are left with a  $2.885 M_{\odot}$  NS with a  $0.2 M_{\odot}$  WD companion in an  $\sim 10$  day orbit. This is typical of the parameters of observed pulsar-HeWD binaries (van Kerkwijk et al. 2004). We have assumed a maximum NS mass of  $3 M_{\odot}$ , however this mass limit is not well constrained. If we were to assume a maximum NS mass of only  $2 M_{\odot}$  the system would end as a WD orbiting a BH.

In terms of pulsar evolution, the magnetic field versus period parameter space covered by the NS is shown in figures 3 and 4 for a variety of parameter value changes. To begin we look at how simply changing the initial period and magnetic field changes the NS particulars over time. We direct the reader to Figure 3 which shows the clear differences in the binary pulsar life if it starts its life with  $P_0 = 2.5 \times 10^{-2}$  s,  $B_{s0} = 5 \times 10^{12}$  G and therefore  $\dot{P}_0 = 9 \times 10^{-13}$  s/s (pluses) or if it starts its life with  $P_0 = 9.3 \times 10^{-2}$  s,  $B_{s0} = 1.4 \times 10^{12}$  G and  $\dot{P}_0 = 2 \times 10^{-14}$  s/s (circles). There is a marked difference between the spin evolution of the pulsars – the evolutionary pathways depend greatly on the strength of the pulsars magnetic field. It is obvious from these curves where accretion began and beyond this the pulsar evolution is similar for the two stars. Comparison can also be made with the isolated pulsar evolution given in the previous example (lower dots), initially these two pulsars evolve similarly until accretion occurs. Another isolated pulsar is shown (higher dots), with  $P_0 = 3.4 \times 10^{-2}$  s,  $B_{s0} = 4.1 \times 10^{13}$  G and  $\dot{P}_0 = 4.9 \times 10^{-11}$  s/s. This isolated pulsar spins down much faster than the other three pulsars (see Figure 3a) and shows the effect a greater magnetic field has on the spin evolution of a pulsar. Once accretion occurs the spin and magnetic field evolution for both binary pulsars changed dramatically. The NSs are eventually spun-up and both possess sub-millisecond spin periods, while the magnetic fields decay rapidly and both reach their lowest limits ( $5 \times 10^7$  G) in  $\sim 30$  years. The  $\dot{P}$  and  $P$  parameter space covered by the three pulsars is given in Figure 3d.

At this stage we have not considered allowing the NS to receive a velocity kick during the SN event. If we allow a large, randomly orientated velocity kick of  $\sim 190$  km/s to occur during the SN then the system is disrupted. However, if a smaller velocity kick is given, say,  $\sim 50$  km/s not only

does the system survive but it passes through a complex set of mass transfer phases including two RLOF phases and a handful of symbiotic phases. The first RLOF mass transfer phase, which began at a system time of 75 Myr, caused the NS to be spun up to 0.02 s, accrete  $0.04 M_{\odot}$  and lasted for 0.2 Myr. The secondary star lost  $4.8 M_{\odot}$  of mass and the separation reduced to  $5.8 R_{\odot}$ . During this phase the magnetic field decayed to its bottom value during the first Roche-lobe phase and the pulsar crosses any assumed death line and can not be observed beyond this evolutionary point.

### 4.3 Binary evolution variations

The examples of binary MSP formation above assumed evolutionary parameters of  $\tau_B = 1000$  Myr,  $k = 10000$  and no propeller evolution. We now reconsider the example with  $P_0 = 2.5 \times 10^{-2}$  s and  $B_{s0} = 5 \times 10^{12}$  G and vary these assumed parameters one at a time. The variations are (see Figure 4):

- Assume  $\tau_B = 5$  Myr (plus symbols within Figure 4);
- Decreasing  $k$  to 0 (circles);
- Allow propeller evolution to occur (crosses);

As expected a lower value of  $\tau_B$  forces the magnetic field to decay rapidly while causing little spin-down of the pulsar spin period to occur. The binary evolution is not noticeably influenced due to this evolutionary change.

Decreasing  $k$  affects the rate of magnetic field decay during accretion (see equation 8) as depicted clearly in Figure 4b. This parameter change seems one we would definitely regard with skepticism because it populates entirely the wrong region of the  $P\dot{P}$  parameter space, in terms of what observation suggest. The binary evolution, again, does not change significantly.

Generally it is thought that if there is going to be a propeller phase it will occur at the beginning of the accretion phase (Possenti et al. 1998), when the pulsar is rotating rapidly enough and the magnetic field is sufficiently large enough. This is what occurs here, however, unlike the propeller phase considered by Possenti et al. (1998), our method causes it to initiate multiple times during this evolutionary example. During the first propeller phase the NS is spun-down, reaching a spin period of  $5 \times 10^4$  s before the phase ends and accretion onto the NS begins. Although the RLOF phase lasts for  $\sim 2000$  Myr – shorter than without a propeller phase – the accretion of mass onto the slowly rotating NS occurs extremely rapidly and unfortunately is only calculated by the BSE over a single time-step. This is the reason for the large ammount of magnetic field decay in one step. Modifying the time-stepping around this region does not affect the evolution greatly, however, it does slow the speed at which we may evolve many systems. The first propeller phase although very efficient in braking the NS spin was short lived, lasting only  $\sim 2.3$  Myr. While beyond the first mass transfer phase the system moved once again into propeller evolution, this time lasting for  $\sim 550$  Myr and spinning the NS down to a  $\sim 1000$  s spin period. Once again, at a system time of  $\sim 580$  Myr the NS accretes material and is spun in one time-step up to  $\sim 0.04$  s spin period. The third propeller phase, initiated directly after the accretion phase, continues until the end of the RLOF mass transfer phase and manages to spin the NS to a period  $\sim 0.08$  s. At the

end of the RLOF phase the companion, now on the first giant branch and  $40 R_\odot$  away from the NS, loses  $\sim 0.001 M_\odot$  of matter the majority of which is collected by the NS. This spins up the pulsar to 0.07 s. We end with a  $0.3 M_\odot$  HeWD, slightly greater than that created without the propeller included. While the NS is  $1.78 M_\odot$ , slightly smaller than when we do not assume the propeller phase to occur.

From the simple analysis above we can see how effective the propeller phase is at braking the pulsar spin. Although the propeller phase arrests the majority of spin-up, and in fact obstructs the formation of a MSP (that would otherwise have formed), it is an important evolutionary assumption to test on populations of NSs. We have also shown that both the accretion-induced field decay parameter  $k$  and the standard magnetic field time-scale parameter  $\tau_B$  are important parameters to regard when modeling the entire pulsar population. We next consider populations of pulsars and how parameter changes affect the morphology of these populations.

## 5 RESULTS AND ANALYSIS

### 5.1 Method

A binary system can be described by three initial parameters: primary mass,  $M$ , secondary mass,  $m$ , and separation,  $a$  (or period,  $P_{\text{orb}}$ ). A fourth parameter, eccentricity, may also vary, however, for simplicity we assume initially circular orbits. For the range of primary mass we choose a minimum of  $5 M_\odot$  and a maximum of  $80 M_\odot$ . To first order this covers the range of initial masses that will evolve to become NSs via standard stellar evolution. Stars below  $\sim 10 M_\odot$  will generally become WDs and stars above  $\sim 20 M_\odot$  will end up as BHs. However, binary interactions tend to blur these stellar mass limits. As suggested in HTP02 the production of stars with  $M > 80 M_\odot$  is rare when using any reasonable IMF, hence the choice of upper mass limit. The lower limit is one that should allow the production of all interesting NS systems to be formed, that is, all systems which have interaction between the NS and its companion. This includes stars with initial masses below  $10 M_\odot$  that accrete mass and form a NS instead of a WD. Expanding the upper limit accounts for stars with  $M > 20 M_\odot$  that lose mass and become a NS instead of a BH. The secondary mass range is from  $0.1 M_\odot$  to  $40 M_\odot$ . The lower limit here is approximately the minimum mass of a star that will ignite hydrogen-burning on the MS. These mass ranges will allow the production of the majority of NS binaries and enable us to investigate complete coverage of the  $P\dot{P}$  diagram. For the initial orbital period we consider a range between 1 and 30000 days. The birth age is randomly selected between 0 and 10 Gyr where the latter reflects an approximate age of the Galaxy.

Instead of calculating birth rates and numbers of systems of interest, our focus, here, is on comparison with the observed pulsar  $P$  vs  $\dot{P}$  diagram and what this can teach us about uncertain parameters in pulsar evolution. These include parameters such as the magnetic field decay time constants in both the isolated and accreting regimes along with the effectiveness of modelling propeller systems to spin-down pulsars to observed periods. We also aim to test how different evolutionary parameter changes affect the relative populations of binary and isolated pulsars.

In distributing the primary masses we use the power law IMF given by Kroupa, Tout & Gilmore (1993),

$$\Phi(M) = \begin{cases} 0.035M^{-1.3} & \text{if } 0.08 \leq M < 0.5, \\ 0.019M^{-2.2} & \text{if } 0.5 \leq M \leq 1.0, \\ 0.019M^{-2.7} & \text{if } 1.0 \leq M < \infty. \end{cases} \quad (26)$$

This is the probability that a star has mass  $M [M_\odot]$ . The distribution of secondary star masses is not as well constrained observationally. We assume that the initial secondary and primary masses are closely related via a uniform distribution of the mass-ratio (Portegies Zwart, Verbunt & Ergma 1997; HTP02),

$$\varphi(m) = \frac{1}{M}, \quad (27)$$

where the mass-ratio ranges from  $0.1/M$  to  $1.0$ . The initial orbital period distribution we take to be flat in  $\log(P_{\text{orb}})$ . Completely sampling these distributions allows us the full range and distribution of initial parameters, so we are modelling the natural selection of stellar systems as suggested by observations.

The results of six simulations (see Table 1) in the form of  $P\dot{P}$  plots are given below (Sections 5.2 to 5.7). These are Models A through F. We begin by simulating a rather naive stellar population (Model A) to which we build pulsar evolutionary phases and assumptions upon in increasingly greater complexity until we feel the results best represent the required pulsar  $P\dot{P}$  parameter space as compared to observations. We note from the outset that we do not attempt to model the slow rotating high magnetic field pulsars in the upper-right region of the  $P\dot{P}$  parameter space. As discussed in Section 6 we leave these potential magnetars for future work. Modifying the assumed initial NS spin period and magnetic field (see Section 5.6) quantifies the importance of choices made in this area. For the most part the initial period and magnetic field ranges (given in Table 1) are selected so as to allow good coverage of the  $P\dot{P}$  parameter space. At this stage we do not suggest that these ranges are completely realistic but we do wish to show that it is possible to produce a complete coverage of the pulsar  $P\dot{P}$  parameter space with them. In Section 5.8 we take Model F and look at some further variations such as inclusion of electron capture supernovae and beaming effects. This includes an examination of the pulsar primordial parameter space (Section 5.8.4) and how changing evolutionary assumptions modifies the pulsar birth properties.

Unless otherwise stated all models have the binary and stellar evolutionary parameters of: solar metallicity  $Z = 0.02$ ; a maximum possible NS mass of  $3 M_\odot$  and  $\alpha_{\text{CE}} = 3$ . SN kicks are given to NSs, while to keep the required number of models down to a minimum we only use the curvature radiation death line model with  $\bar{f}_{\text{prim}}^{\text{min}} = 0.15$ . Although we know the CR death line to be insufficient in terms of modelling recycled pulsars it is adequate for our purposes here (for more see Section 6). For each model we evolve  $10^7$  primordial systems, all of which are initially binary systems. Integrating over the Kroupa, Tout & Gilmore IMF with the mass limits set above, modeling  $10^7$  primordial systems is roughly representative of  $2 \times 10^9$  systems in the Galaxy if the full mass range is allowed. One way to think of this is that we are assuming a stellar birth rate of  $10^{-3}$  systems/year,



assuming the age of the Galaxy is 10 Gyr. In mass, we are only evolving  $\sim 0.1\%$  of the Galaxy assuming it contains  $\sim 1 \times 10^{11} M_{\odot}$ . This is something that in the future we will wish to increase.

## 5.2 A starting model

We start by demonstrating the results of pulsar population synthesis when no field decay owing to the accretion of material onto a NS is allowed. This is done by setting  $k = 0$  in Equation 8. The result is Model A for which the pulsar evolutionary parameters are given in Table 1 and the  $P\dot{P}$  distribution is shown in Figure 5. Clearly from Figure 5 there are a great number of rapidly rotating pulsars with large spin period derivatives. This is not observed which means that this model fails to decay the magnetic field quickly enough during accretion. Therefore, Model A seems physically unrealistic. One may be skeptical of this result based on one model, however, similar  $P\dot{P}$  distributions occur even if we vary additional parameters such as  $\Xi_{\text{wind}}$  (to lower the angular momentum transferred during accretion) and/or using lower values of  $\tau_B$ . It is interesting to observe the different levels of pulsar densities in the spun-up region of Figure 5 – there is almost a wave-front effect towards MSP periods. The pulsars in these regions have differing companion types and orbital configurations indicating different mass transfer histories. Here the fastest rotating pulsars generally have MS companions and circular orbits. In these cases mass transfer occurs via RLOF. For the pulsars located in the spin-up region truncated at  $P \sim 0.002$  s companion types are mainly giant and white dwarfs and include many cases of eccentric orbits. This indicates mass transfer via a stellar wind from a giant star in a binary with a relatively long orbital period. Systems which have a shorter orbital period and initiate RLOF from a MS companion can accrete a greater amount of material and hence are spun-up further to left in the  $P\dot{P}$  diagram.

## 5.3 Magnetic field decay during accretion

Model A shows that some form of accretion induced magnetic field decay is required to suitably populate the recycled region of the  $P\dot{P}$  diagram. A first attempt at modelling this physics is completed in Model B (see Table 1), where we  $k = 10000$  in Equation 8. The resultant  $P\dot{P}$  parameter space is shown in Figure 6. This simulation gives good coverage of the observed pulsar regions – the standard and recycled islands. However, there is an over-production of systems linking the two pulsar  $P\dot{P}$  islands. Many of these pulsars are paired with early type stellar companions (pre-degenerate stars) with strong winds that may disrupt the radio beam (see Section 5.8.2). A number of these systems are also beyond what is considered the general ‘spin-up’ line. The spin-up line is a theoretical construct which suggests that an accreting pulsar will eventually reach some equilibrium spin period and therefore end pulsar spin-up during the accretion phase. The spin-up line, however, is a very uncertain model and the majority of assumptions that go into it are highly variable (see Arzoumanian, Cordes & Wasserman 1999 and references therein for details), and the line is sensitive to changes for many parameter values. We do not directly impose the spin-up line in our models but instead aim

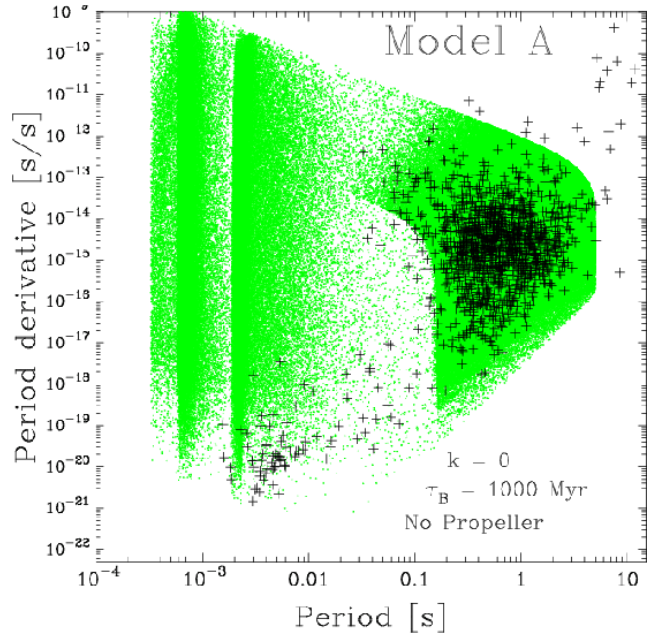


**Figure 5.** The  $P\dot{P}$  diagram for Model A. The relevant parameter values are given in Table 1 and on the figure. Plus symbols represent the observed pulsars, while grey dots represent each pulsar the simulation produces.

to have its effect replicated by the physical processes that make up our binary/pulsar evolution algorithm. As such we would clearly want to limit the production of medium-low period high- $\dot{P}$  pulsars that appear in Model B. This is a motivator for testing the affect of including propeller physics. One may also notice the line of MSPs at the bottom right of Figure 5. This line appears in all the  $P\dot{P}$  figures shown here and is caused by the assumed limit of magnetic field decay (Section 3.6).

## 5.4 Propeller evolution

Propeller evolution (Section 3.3) is permitted in Model C, which is otherwise the same as Model B. The results are shown in Figure 7 which exhibits three main features that make modelling the propeller evolution beneficial. The first is the slight bump from the standard pulsar island in slower spin period pulsars ( $P > 5$  s). This slight bump is directly caused by the propeller phase, and allows us to model those pulsars who reside next to the standard pulsar island. Although, we note that those pulsars could also be modelled if we assume that the magnetic field does not decay other than during accretion. The second feature of interest is the cut off of millisecond pulsars with period derivatives between  $10^{-21}$  and  $10^{-18}$ , as compared to Model B. Although this cut-off occurs too soon (in terms of pulsar period) it does provide a method for producing this observed limit in period. The third feature is lack of pulsars with period derivatives between  $10^{-16}$  and  $10^{-13}$  and spin periods of around 0.01. Therefore, when considering  $P\dot{P}$  parameter space, we find that including the propeller phases provides much better agreement with models that impose a spin-up line directly to restrict pulsars appearing above the observed pulsar bridge.



**Table 1.** Characteristics of the main set of models used in this work. The first column gives an identifying letter for each model. Within the second column we indicate the value of the magnetic field decay time-scale which is followed by the choice of accretion induced magnetic field decay parameter. The fourth and fifth columns indicate whether or not propeller evolution is considered and whether a link between SN strength and initial magnetic field and pulsar period is assumed. The next four columns indicate the maximum and minimum values for the initial distributions of pulsar spin period and magnetic field. We then modify the ammount of angular momentum accreted by a NS when the companion is losing mass in a wind, this is governed by the parameter  $\Xi_{\text{wind}}$ . The penultimate column indicates if the electron capture SN kick distribution is considered and the final column indicates whether beaming and accretion selection effects are considered.

Model	$\tau_B$ [Myr]	$k$	Propeller	SN link	$P_{0\text{min}}$ [s] <sup>a</sup>	$P_{0\text{max}}$ [s]	$B_{0\text{min}}$ [G]	$B_{0\text{max}}$ [G] <sup>b</sup>	$\Xi_{\text{wind}}$	EC SN	Beaming
A	1000	0	No	No	0.01	0.1	$1 \times 10^{12}$	$3 \times 10^{13}$	1	No	No
B	1000	10000	No	No	0.01	0.1	$1 \times 10^{12}$	$3 \times 10^{13}$	1	No	No
C	1000	10000	Yes	No	0.01	0.1	$1 \times 10^{12}$	$3 \times 10^{13}$	1	No	No
D	5	10000	Yes	No	0.01	0.1	$1 \times 10^{12}$	$3 \times 10^{13}$	1	No	No
E	2000	3000	Yes	Yes	0.02	0.16	$5 \times 10^{11}$	$4 \times 10^{12}$	1	No	No
F	2000	3000	Yes	Yes	0.02	0.16	$5 \times 10^{11}$	$4 \times 10^{12}$	variable	No	No
Fb	2000	3000	Yes	Yes	0.02	0.16	$5 \times 10^{11}$	$4 \times 10^{12}$	variable	Yes	No
Fc	2000	3000	Yes	Yes	0.02	0.16	$5 \times 10^{11}$	$4 \times 10^{12}$	variable	Yes	Yes
Fd	2000	3000	No	Yes	0.02	0.16	$5 \times 10^{11}$	$4 \times 10^{12}$	variable	No	No

<sup>a</sup> For the SN link models this value is the average initial spin period  $P_{0\text{av}}$ , not the minimum.

<sup>b</sup> For the SN link models this value is the average initial magnetic field  $B_{0\text{av}}$ , not the maximum.

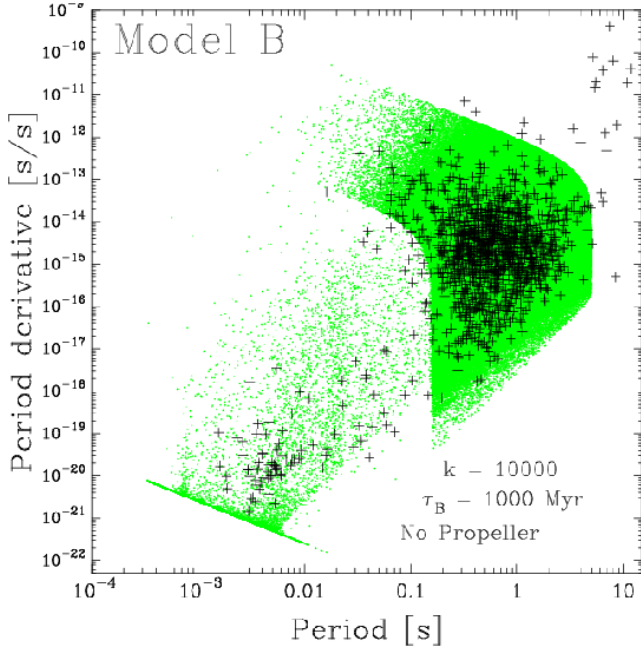


**Figure 6.** The  $P\dot{P}$  diagram for Model B. The relevant parameter values are the same as Model A except for the accretion induced field decay parameter which is now  $k = 10000$ . Plus symbols represent the observed pulsars, while grey dots represent each pulsar the simulation produces.

### 5.5 Magnetic field decay timescale

Model D differs from the evolutionary assumptions in Model C by assuming  $\tau_B = 5$  Myr (reduced from 1000 Myr). This rapid field decay has the effect of shifting the standard pulsar island to the left in the  $P\dot{P}$  diagram (see Figure 8). Even so, looking at Figure 8 we see it is not possible to properly simulate the standard pulsar island with  $\tau_B = 5$  Myr, unless a completely contrived initial period range is used. Also in Figure 8 it is noticeable that even before consideration of

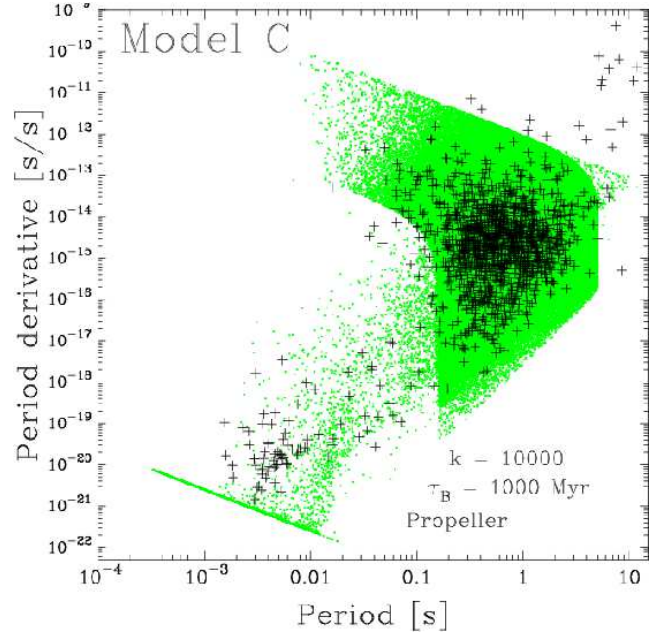


**Figure 7.** The  $P\dot{P}$  parameter space for Model C. Plus symbols represent the observed pulsars, while grey dots represent each pulsar the simulation produces.

selection effects there is a large underproduction of recycled pulsars. The rapid field decay causes the majority of spun-up pulsars to sit on the lower magnetic field limit, a region of the  $P\dot{P}$  parameter space in which any complete death line model should remove. As such, assuming such a low value of magnetic field decay, as has been used in the past by Gonthier et al. (2002), for example, is unrealistic. We find that  $\tau_B$  of 100 Myr or greater is required to produce a reasonable  $P\dot{P}$  distribution.

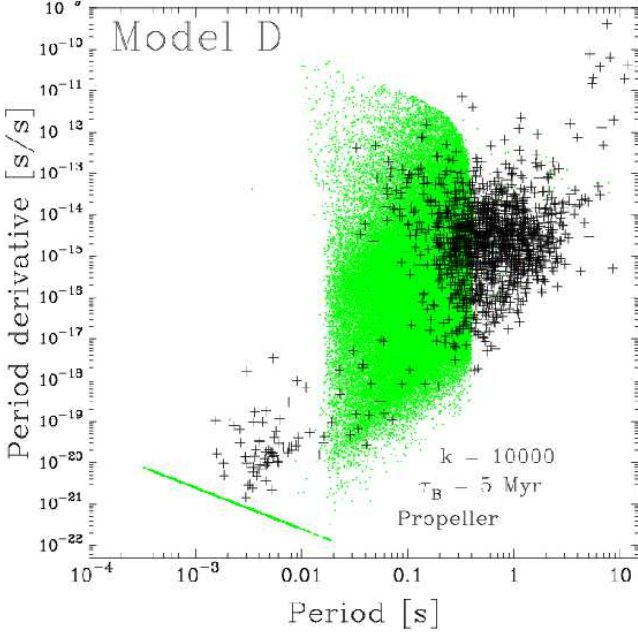


**Figure 8.** The pulsar  $P\dot{P}$  parameter space for observed and those simulated pulsars produced by Model D. This facilitates comparison between a large and small  $\tau_B$  when compared to Figure 7. Plus symbols represent the observed pulsars, while grey dots represent each pulsar the simulation produces.

### 5.6 Updated initial pulsar distribution: SN link

With the propeller phase producing what seems to be a more realistic population in Model C than that which occurred in Model B, while also constraining  $\tau_B \geq 100$  Myr in Model D, we now conduct a trial to see what effect linking the SN velocity kick magnitude with the initial period and magnetic field (see Section 3.4) has on the pulsar distribution in  $P\dot{P}$ . To do this we make use of equations 15 and 16, assuming  $n_p$  and  $n_b$  are unity. The corresponding values of  $P_{0av}$  and  $B_{0av}$  are given in Table 1 (see Model E). Note that the distribution of initial pulsar period and magnetic field is modified (as compared to Models A through C) to allow better coverage of the standard pulsar island in the observed  $P\dot{P}$  space. The value of the lower initial magnetic field limit,  $B_{s0min}$ , was used due to suggestions that there are NSs which are born weakly magnetised ( $\sim 5 \times 10^{11}$  G; Gotthelf & Halpern 2007). We also allow a greater coverage of the slower rotating pulsars by assuming  $\tau_B = 2000$  Myr. The previous value of  $\tau_B = 1000$  Myr under populated the slower pulsars when used in conjunction with this model. Conversely if the value of  $\tau_B$  is greater than 2000 Myr the lower region of the standard pulsar island is increasingly truncated – the magnetic field decays too slowly to sufficiently decrease the period derivative. These changes result in Model E and its  $P\dot{P}$  diagram is shown in Figure 9. There are now striking similarities between the observed and simulated  $P\dot{P}$  parameter spaces, particularly at the standard pulsar island. Three main features in Figure 9 of worthy note are as follows: (1) the production of a wall of young pulsars, which indicates that those pulsars born with strong magnetic fields also initially spin at a faster rate to those born with lesser magnetic fields (which is what we expect from Equations 15 and 16); (2) the only method for pul-

sars to have periods of  $\sim 4$  seconds or slower, in this model, is to pass through a propeller phase; and (3) the observed group of high  $P$  ( $\sim 10^{-14} - 10^{-12}$  [s/s]) but moderately rapid rotating pulsars ( $\sim 0.01 - 0.2$  [s]) are reasonably well modelled. It should be pointed out here that within Model E there is a different reason why the  $P\dot{P}$  area described in point three is populated as compared to the explanation given for Figure 1. Within Model E these systems arise due to mass transfer, while the assumed formation mechanism of these pulsars (for Figure 1) was that these were newly formed NSs and born there.

In terms of the shape of the  $P\dot{P}$  parameter space, we are able to simulate some regions of the observations rather accurately. To begin we only slightly over-estimate the cut-off of pulsars at small spin periods. This cut-off arises from a combination of the assumption of  $k$  and the propeller evolutionary phase. The death line does a satisfactory job at limiting the semi-recycled pulsars however it fails in limiting both the slower rotating pulsars and the fully recycled pulsars. This failure is not unexpected because the curvature radiation death line is not a completely realistic model when considering the full pulsar population (see Section 6 for further discussion on this point).

What is not noticable in Figure 9 is the number of pulsars that evolve through a Thorne-Żytkow object phase. As explained earlier a TZO is a remnant core (NS or BH) surrounded by an envelope formed from the non-compact star with which it has merged. In BSE these objects are treated as unstable so that the envelope is ejected instantaneously. However, we are left with the question of what to do with the pulsar parameters. For now we keep this evolutionary phase consistent with our CE phase were we assume that the spin period and magnetic field are re-set by this process. This assumption is preferred at this stage because if we assume the pulsar is left unchanged we find many isolated pulsars rotating near their assumed break-up spin velocities ( $P \sim 4 \times 10^{-4}$  s) with a large range of spin period derivatives ( $\dot{P} < 10^{-15}$ ). We note here that our assumption regarding these objects is purposefully simplistic to reflect our lack of knowledge about what occurs during the formation and evolution of a TZO but other possibilities are discussed in Sections 5.8.2 and 6.

Once again, there is an over production of pulsars above the observed pulsars which link the two pulsar islands. In the next section we again increase the detail of our model in an attempt to constrain this  $P\dot{P}$  region.

### 5.7 Testing wind angular momentum accretion, the $\Xi_{wind}$ parameter

The effect of modifying  $\Xi_{wind}$  (Model F) is shown in Figure 10 and is dramatic when compared with Figure 9. This modification truncates the width of the pulsar bridge which was the aim of this model. The pulsar bridge that stretches between the two pulsar islands compares rather accurately to the observations (in terms of  $P\dot{P}$  area covered). This is our preferred model and we now perform an in depth analysis of this model, including further parameter changes (see Table 1).

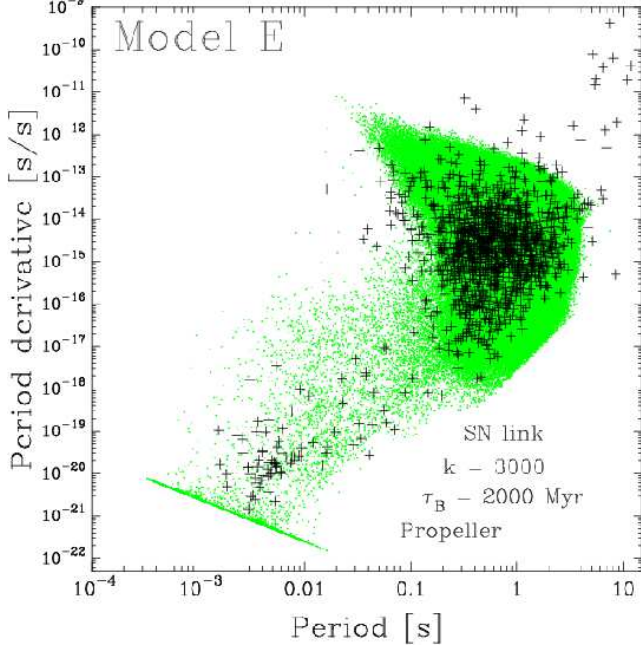


**Figure 9.** The pulsar  $P\dot{P}$  parameter space for Model E. Plus symbols represent the observed pulsars, while grey dots represent each pulsar the simulation produces.

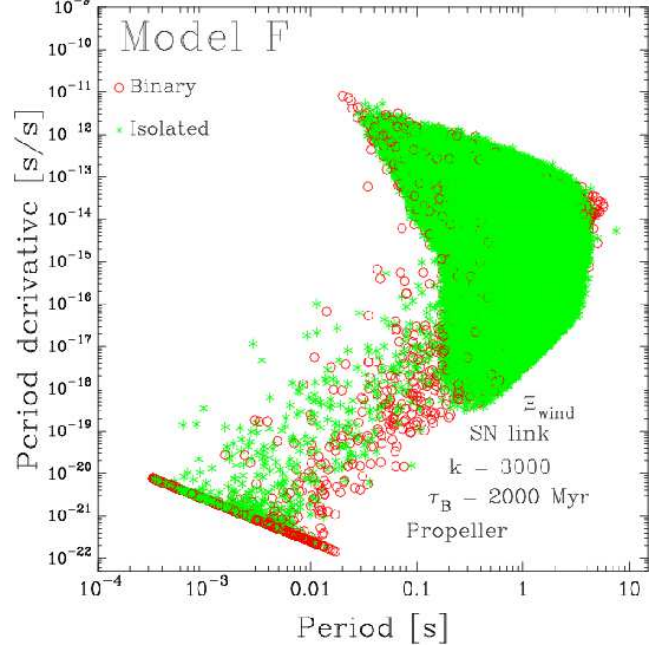


**Figure 11.** The binary (circles) and isolated (stars) pulsar  $P\dot{P}$  parameter space for Model F.

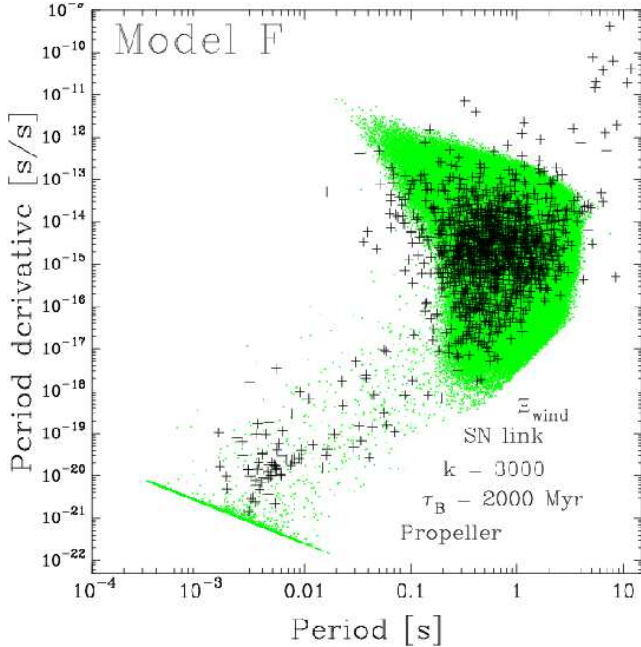


**Figure 10.** The pulsar  $P\dot{P}$  parameter space for Model F. Plus symbols represent the observed pulsars, while grey dots represent each pulsar the simulation produces.

### 5.8 Model F: analysis and further additions

Before we embark on our further examination of Model F we must remind the reader that – at this stage – our parameter space analysis is incomplete. Therefore, although we provide evidence for the formation of such systems as: isolated MSPs, eccentric double neutron stars and possible existence of Galactic disk eccentric MSP-BH binaries;

we must stress that it is possible for many realistic model parameter changes to modify the resultant formation probability of these systems. However, we provide this section as an example of typical binary, stellar and pulsar features that our future complete pulsar population synthesis package will be able to constrain when one is able to compare theoretical results directly with observations. This section also provides evidence of how some evolutionary assumptions further modify the final pulsar population.

Figure 11 depicts the isolated and binary pulsar systems in the  $P\dot{P}$  parameter space for Model F. Focusing on MSPs, the relative number of binary to isolated MSPs is 0.49. Note that we are restricting our comparison to those pulsars that have a magnetic field greater than  $6 \times 10^7$  G and less than  $1 \times 10^9$  G (model pulsar period region is  $P < 0.02$ ; see Figure 1 for observational comparison). In doing this we are ignoring those pulsars that sit on the bottom magnetic field limit. To examine the MSP population of Model F in further detail we show the initial primary and secondary mass distributions of the isolated and binary MSPs in Figure 12a and see that these differ. Notably the average initial mass of the secondary stars is typically greater for binaries that go on to produce isolated MSPs. What this is showing is that the isolated MSPs are passing through two SN events and it is the second SN that disrupts the system. This provides us with a simple method for producing isolated MSPs rather than requiring the addition of some ad-hoc model where the MSP is destroying the companion. This suggested formation mechanism of isolated MSPs is not restricted to Model F alone but to all models completed so far, in fact, due to our restriction of the accreted wind angular momentum we are now producing less isolated MSP systems than previously. Therefore, we believe this is an important evolutionary phase that should be placed under further scrutiny within the community.



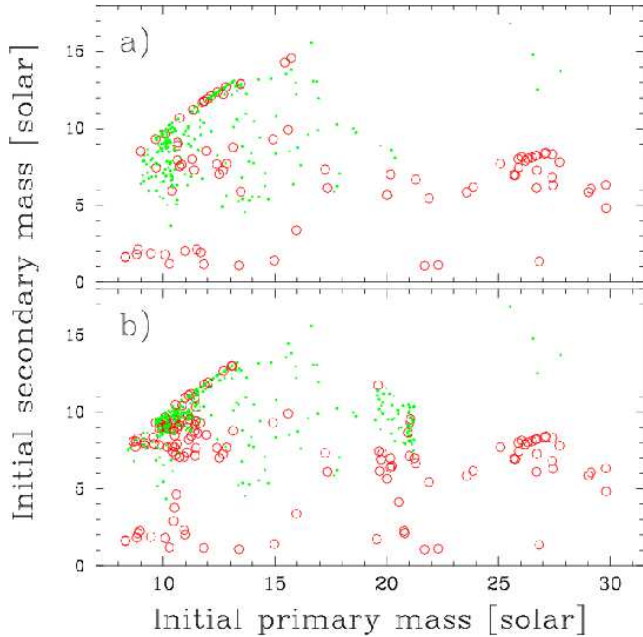


**Figure 12.** The binary (circles) and isolated (dots) MSP initial mass parameter space for Model F in a and Model Fb in b. All systems here fulfill the  $6 \times 10^7 \leq B_s \leq 1 \times 10^9$  G and  $P < 0.02$  criterion.

A number of these disrupted MSPs arise from systems which contain initial secondary masses lower than the assumed upper mass limit for the EC SN model as shown in Figure 12. This suggests that if we allow EC SNe and adopt the associated lesser  $V_\sigma$  value (see Section 3.5) that many of the now isolated MSPs may retain their binary companion. This leads us to consider the effect the combined EC SN and standard SN velocity kick distribution has on our model pulsar population.

#### 5.8.1 A new supernovae velocity kick distribution: electron capture supernovae

We have repeated Model F with the electron capture SN kick distribution taken into consideration to produce Model Fb. We find that Models F and Fb do not differ greatly from each other in terms of the regions of the  $P\dot{P}$  parameter space covered (hence we do not show Model Fb). Surprisingly the binary to isolated MSP ratio has only risen to 0.53 in comparison to Model F. However, Model Fb does contain a greater number of binary MSPs. The initial mass parameter range of MSPs that arise in Model Fb is shown in Figure 12b). It is obvious that many more binary MSP systems are now being born in and around the  $\sim 10 M_\odot$  primary mass and  $\sim 7 - 10 M_\odot$  secondary mass range as expected. Not so expected was the number of newly formed isolated MSPs that are also derived from this primary and secondary mass region. It appears that many primary mass stars are forming NSs via the electron capture method, allowing them to remain within a binary system and receive angular momentum from their companion which then also goes SN, disrupting the system. In particular as Figure 12b) shows, there are a greater number of isolated (and binary) MSPs being born from the  $20 M_\odot$  primary mass region than

in Model F (Figure 12a). A thorough analysis of the ECSN model can not be completed at this stage as considerations of NS space velocities are required for any complete examination of this assumption. However, we have demonstrated some effects the ECSN model imparts on the pulsar population. As such it seems likely that the EC assumption will play an important role in future NS population synthesis works. Especially if comparison to observations of orbital period, eccentricity and space velocities are attempted.

#### 5.8.2 Beaming effect and accretion: a start on selection effects

The source of radio emission from a pulsar occurs at the magnetic poles, otherwise known as the polar caps. The radio waves are well collimated and form a beam. This beam sweeps across the sky (as observed from the pulsar) and may be observed if the beam crosses the observer line of sight. Some regions of the pulsar sky are not covered by the beam – the beaming effect considers the chance that a particular pulsar is beaming across our line of sight. Tauris & Manchester (1998) examined this and found the fraction  $f(P)$  of pulsars beaming towards us in terms of pulsar spin period,

$$f(P) = 0.09 (\log(P) - 1)^2 + 0.03. \quad (28)$$

This equation shows that the faster the pulsar rotates the greater the chance that it is beamed towards us. The basic reason for this is that the pulsar cap angle (beam size or beam angle) is larger for fast rotators. A full explanation relies on details of the magnetic field and beam emission mechanism and we suggest the reader consider Tauris & Manchester (1998). However, the pulsar still may not be observed if selection effects conspire against our observing it. In fact there are some systems that we can rule out directly as not being observable in the radio regime. These are accreting systems or those in which the companions wind is energetic (Illarionov & Sunyaev 1975; Jahan-Miri & Bhattacharya 1994; Possenti et al. 1998). Thus, using Equation 28 we ignore those pulsar that are beamed away from us in combination with ignoring those that have a non-degenerate companion (including stars on the main sequence, although this may be too strict and could possibly be relaxed), or a pulsar which is accreting material. We also assume that it takes time for a pulsar to be observed (at radio wavelengths) after the end of an accretion phase – here we assume it takes 1 Myr. Furthermore, any system which passed through a TŻO phase is considered to be unobservable owing to the ejected nebulous material inhibiting radio transmission. Model Fc results from these considerations.

Because this model only culls the number of pulsars in the  $P\dot{P}$  parameter space we do not show a comparison figure. It is reassuring that the inclusion of beaming does not alter the good agreement found between the model and the observations in terms of the  $P\dot{P}$  diagram. With the inclusion of beaming and the assumption that pulsars can not be observed for some time after accretion we find the binary/isolated MSP ratio is 0.38 for Model Fc with the majority of MSPs produced by wind accretion.

### 5.8.3 Propeller physics appraisal

Here we examine further the effect propeller physics (described in Section 3.3) has on the pulsar population. Motivation for this arises from the lack of binary MSPs coming from the RLOF channel in Model Fc. This arises because the propeller phase halts and then reverses the majority of spin-up phases (as seen in Figure 4). In other words, many Roche-lobe overflow NS systems are having their spin-up phases truncated at some medium to slow spin period and therefore are not being ‘observed’ by BINPOP as they reside below the death line within the  $P\dot{P}$  parameter space (at spin periods of  $\sim 0.03$  or slower). This is in stark contrast to the standard method of assumed MSP formation, which is thought to occur via a low-mass X-ray binary phase (see Section 1 and references therein; although see also Deloye 2007 for an interesting discussion on the low-mass X-ray binary-MSP connection). This result begs the question ‘what would these later models (that is, say, Model F) produce if propeller evolution was not included?’. To answer this we have repeated Model F with the propeller option turned off to create Model Fd.

In comparison to Model F we find that the  $P\dot{P}$  parameter space of Model Fd is similar, the most notable exception being a slight increase in the width of the pulsar bridge (in  $P$ ). We certainly feel it is a plus to have the propeller option in our evolution algorithm, especially when one considers the claims of Winkler (2007), who suggests a new class of high-mass X-ray binary with the massive companions losing mass in winds yet the NSs have spin periods of order 100–1000 s. Conversely, observations of X-ray binaries that contain a rapidly rotating NS, including the growing range of observed millisecond X-ray powered pulsars (Galloway 2007; Krimm et al. 2007), which we can produce in Model Fd, confirm that care must be taken when implementing propeller evolution. This suggests that improvements are required in how, and to what extent, propeller evolution is modelled. Our work presented here also corresponds to the claims made by Kulkarni & Romanova (2008). They show that unstable transfer of mass onto the accretor may occur – even during stable mass transfer events. Therefore, further investigation in this area is required, especially with regard to the possibility of transient pulsar mass accretion in X-ray binaries.

It is interesting to note that with the increased number of RLOF binary MSPs in Model Fd that the binary/isolated ratio is 1.6. This compares well to the observed ratio (Huang & Becker 2007). However, it is too early on in our study to make conclusions based on such a comparison and there may well be a set of parameter changes that affect this result that we have yet to consider.

### 5.8.4 Primordial parameter range

Up until now the majority of our focus has been on pulsar evolution and how modifying the parameter values used in the assumed evolution of pulsars affects the distribution of pulsars that are produced. However, one of the advantages in coupling pulsar evolution with a full binary evolution algorithm is that it allows us to quantify the range of initial binary parameters from which pulsars and particularly MSPs are generated. It also facilitates the investigation of how uncer-

tain assumptions in binary evolution affect these ranges and the nature of the pulsar population.

In Figure 13 we show the distributions of initial binary parameters that lead to pulsar production in Models B, Fb and Fc. In these distributions we consider only those pulsars that are plotted in their respective model  $P\dot{P}$  diagrams – that is only those pulsars above the death line and for Model Fc those pulsars that satisfy the assumed selection effects. Also, a binary system is only considered once, even if that system produces two pulsars in the observable  $P\dot{P}$  region (although this is relatively rare). We also include pulsars that lie on the lower magnetic field limit. All three primary mass distributions peak at around  $8 M_{\odot}$ . This value is the minimum mass in which a star is guaranteed to form a NS (based on the stellar evolution algorithm). As we have addressed previously (Section 3.5), the production of a NS from stars in the  $\sim 6\text{--}8 M_{\odot}$  primary mass range will depend upon the evolutionary pathway, particularly any associated mass loss/gain. The drop off at around  $11 M_{\odot}$  in the mass distributions is chiefly a stellar evolution feature – for solar metallicity models stars with  $M > 11 M_{\odot}$  ignite core-helium burning before the giant branch which gives a change in the radius evolution and stellar lifetime. Formation of NSs with primary masses less than  $6 M_{\odot}$  can only occur via mass accretion or coalescence. The difference in the peak in and around  $8 M_{\odot}$  between Model B and Fb is due to propeller evolution. Those NSs that accrete mass and go on to collapse further into BHs, in Model B, instead accrete less material due to the propeller phase in Model Fb and thus live longer lives as NSs and as such are more likely to be ‘observed’ within BINPOP. Although not examined in much detail here, at first glance one may consider this process to have a highly detrimental effect on the birth rate of BH low mass X-ray binaries when compared to NS low mass X-ray binaries (see Kiel & Hurley 2006 for discussion). However, because the NS is in a propeller phase for up to hundreds of millions of years – and will not be counted as a NS low mass X-ray binary during this time – these systems will not add greatly to the birth-rate calculations of these X-ray systems. In comparison to Models B and Fb, Model Fc produces a lower number of pulsars, as expected. The distribution of secondary masses for all three models peaks at around  $5 M_{\odot}$  and covers the range from  $0.1\text{--}33 M_{\odot}$ . This peak is due to a combination of the lower limit of  $5 M_{\odot}$  for primary stars, the fact that dynamic or long lived mass transfer events occur most often in binary systems in which the mass ratio is near unity and that the coalescence of two  $\sim 5 M_{\odot}$  stars leaves one that is able to form a NS. Finally we come to the orbital period distribution where we find that short orbital periods are favoured. Bearing in mind that the initial distribution of periods is flat in  $\log P$ , and thus, the relative number of binary systems born with periods in the  $1\text{--}10$  d and  $10\text{--}100$  d ranges are the same, it is interesting to see that the period distribution of pulsar progenitors does not follow that of all binaries. This indicates that close binary evolution is instrumental in increasing the number of observable pulsars. With the advent of detailed pulsar evolution in combination with rapid binary evolution it is now possible (as demonstrated here) to consider the underlying main sequence stellar population that generates the complete observed radio pulsar distribution.

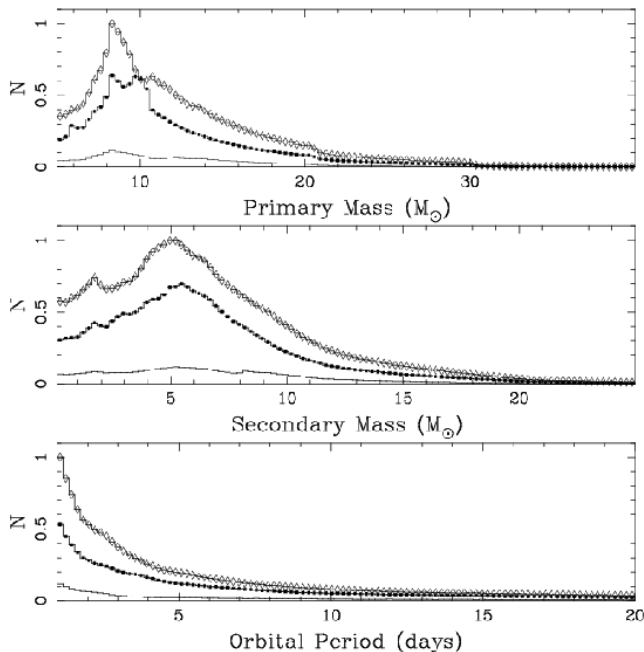


**Figure 13.** Pulsar primordial parameter space distributions for primary mass, secondary mass and orbital period. The full squares represent the distribution of Model B, diamonds Model Fb and the plain line Model Fc. Distributions are normalised to the maximum of each parameter across the three models.

#### 5.8.5 Observational constraints and predictions

Conclusions on how complete our knowledge truly is for aspects of binary evolution theory may be drawn if we compare certain pulsar population features directly with observations. This may be completed in some limited form even though we do not yet consider selection effects fully. To do this we explore in greater detail the accretion physics at play in Model Fd. In particular, we examine MSP mass accretion showing that under standard accretion physics assumptions the RLOF-induced MSPs accrete enough material for their magnetic fields to decay beyond observed values (in this model we assume a bottom field of  $5 \times 10^7$  G). Figure 14 shows that many MSPs that were spun-up via RLOF accreted greater than  $\sim 0.1 M_\odot$  worth of mass. Which, according to the prescription presented here is enough accreted material to decay/bury the field. In fact we find that  $\sim 0.004 M_\odot$  is enough mass for a NS to accrete and sit on or close to the bottom field, or if we assume no bottom field it is enough mass that the NS will not be observable as a pulsar. We note that the MSP spin periods calculated in this work should be considered lower limits. The BSE algorithm takes care to conserve angular momentum and the spin period resulting from the accretion of material is based on the angular momentum transferred by the material. We also perform a check that this does not violate energy conservation (which affects the lower left-hand region of Figure 14), however, this check currently assumes that all the gravitational potential energy of the accreted mass is converted into rotational energy for the accreting star. Refining this treatment will be investigated further in the future.

We also consider the mass range of pulsars produced in the above suggested model and compare this with observa-

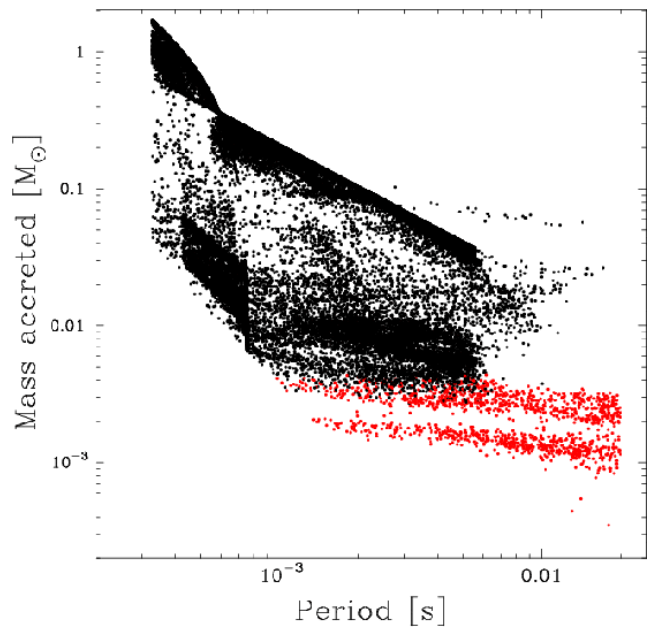


**Figure 14.** Mass accreted since SNe for all pulsars rotating with spin periods faster than 0.02 s excluding those that fail our energy conservation check (see text for details). These pulsars are formed from Model Fd (with out propeller physics included). Black points represent those unobservable pulsars whose magnetic field has decayed to the assumed bottom magnetic field limit. All other points represent potentially observable MSPs.

tions. Figure 15 depicts the distribution of NS mass against spin period and provides the number density of pulsars over the entire mass range. Note that in our models we assume a maximum NS mass of  $3 M_\odot$ , which explains the upper cut-off in the mass distribution (and also affects how much mass a NS can accrete before becoming a BH). Overlaid on our model mass distribution is the observed pulsar masses with their errors as quoted from Table 2 of Nice (2006; and references therein) and Table 1 of Freire (2007; except for pulsar J1748-2021B). We also include the latest mass estimate of MSP J0437-4715 by Verbiest et al. (2007) and updates of J0705+1807, J0621+1002 and J1906+0746 from Nice, Ingrid & Kasian (2008), while we make use of Lattimer & Prakash (2007) for pulsars J0045-7319 and J1811-1736. At this stage, due to the lack of observational constraints, we believe it would be inadvisable to put forward strong views on this matter. It is also instructive to see what occurs if we ignore those MSP-like NSs that would most likely be unobservable due to accretion induced field decay (again see Figure 15). We see that a large number of the highly recycled pulsars are now removed from the mass distribution. When only considering those potentially observable re-cycled NSs the apparent overlap of observed to theoretically produced pulsars, in the spin period  $\sim 0.003$  to  $0.01$  range, is now more prominent. Beyond this spin range the number density of observable model pulsars drops off somewhat.

In keeping with our discussion on MSPs we now consider what MSP companion types are produced by Model Fd and the ratio of eccentric to circular orbits in MSP binaries. MSP binary systems comprise much of the interesting binary evolutionary phases in their histories and as such will play an important role in constraining binary and stellar evolu-



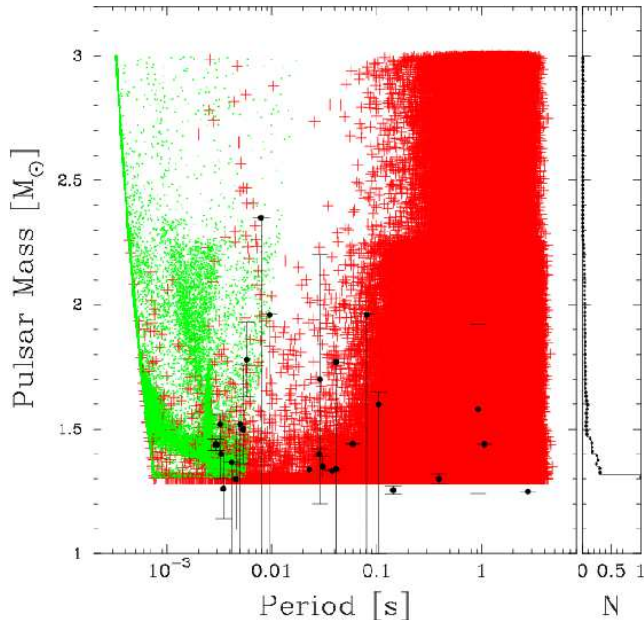


**Figure 15.** NS mass versus spin period for the complete population of Model Fd. Plus symbols represent NS formed from our model with  $B_s > 6 \times 10^7$  G (and thus potentially observable) while the light dots represent all other model pulsars. The darker points show observations and their suggested errors. On the right we show the density of pulsar mass. We see that the majority of pulsars have masses in the range 1.3 to 1.5  $M_\odot$ .

tion theory via population synthesis. Figure 16 depicts our Model Fd MSPs in the eccentricity-orbital period parameter space. The model MSPs in Figure 16 are selected to have  $B_s > 6 \times 10^7$  G and spin periods less 0.02 s. Model Fd is also able to produce eccentric WD-MSP systems although the most eccentric of these systems in which the MSP is not in the process of accreting material is one with an eccentricity of 0.2. All eccentric MSP-MS binary systems depicted within Figure 16 are also accreting and thus not observable as radio pulsars. It is interesting to note the healthy amount of double NS systems Model Fd produces which include a millisecond pulsar and a large eccentricity. As an example to the extent of predictive power our future code will have on the possible understanding or interpretation of observations, we now consider the MSP J0514-4002A (Freire et al. 2004). This is the observed binary system depicted in Figure 16 with an eccentricity of 0.888. At present this binary system has a measured mass of  $M_{\text{system}} = 2.453 M_\odot$  and resides within the globular cluster NGC 1851. The MSP, which rotates at  $P = 0.004991$  s, has an estimated mass of  $< 1.5 M_\odot$  which leads Freire, Ransom & Gupta (2007) to argue that the minimum mass of the companion is 0.91  $M_\odot$ . This being the case Freire, Ransom & Gupta (2007) suggest that the companion is a heavy WD and that the most likely formation mechanism is via third body interaction due to the globular cluster high stellar density. Although the likelihood of this formation mechanism being the correct one is high they do suggest an alternative – a near head-on collision of a pulsar and giant star. However, because of where J0514-4002A sits within Figure 16 we consider a different possible binary companion type and formation mechanism for J0514-4002A. Some of the highly eccentric MSPs clustered around

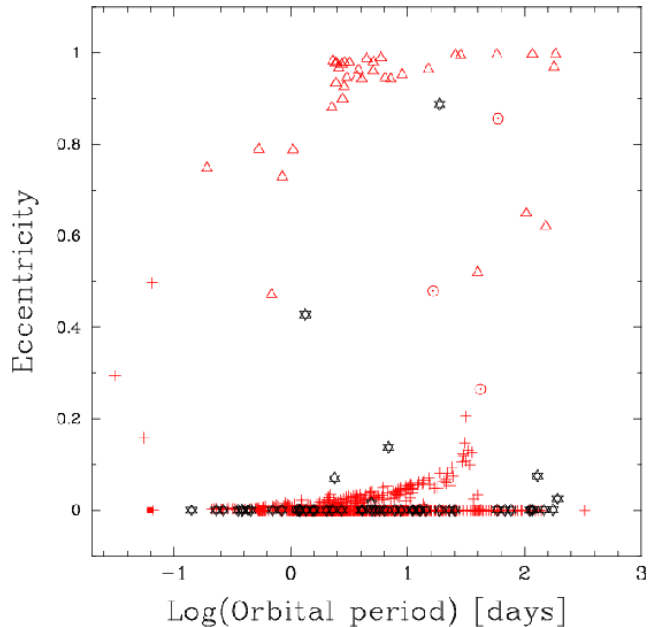


**Figure 16.** MSP eccentricity versus orbital period for the MSP population of Model Fd. All pulsars here have magnetic fields such that  $B_s > 6 \times 10^7$  G and spin periods less 0.02 s. Triangles represent model double NS systems containing one MSP. Plus symbols are WD-MSP systems,  $\odot$  symbols represent main sequence-MSP systems while solid squares represents naked helium-MSP systems. There are not many naked helium-MSPs within this figure and all of them reside in circular orbits, thus rendering them hard to see. The black stars are observed pulsars taken from the ATNF pulsar catalogue (Manchester et al. 2005).

$1 < P_{\text{orb}} < 10$  days within Figure 16 have low mass primary and secondary NSs, that is  $M_{\text{system}} < 2.7 M_\odot$ . The MSPs within this region have accreted only  $\sim 10^{-3} M_\odot$  and have been spun-up to periods,  $2 \times 10^{-3} < P < 10^{-2}$  s. So, we have some low mass systems which roughly fit the observed binary system containing MSP J0514-4002A, bearing in mind that our minimum initial NS mass is 1.3  $M_\odot$ . This is especially the case if one assumes a minimum NS mass of  $\sim 1.2 M_\odot$  – the latest minimum pulsar mass estimate (Faulkner et al. 2005). Prior to this it was assumed that pulsar masses were greater than 1.3  $M_\odot$  – the value which BSE was calibrated to. This is something that will need to be revised in the future. Therefore, the model suggests that a low-mass highly eccentric MSP-NS system should also be considered as a possible explanation for this binary (in addition to the eccentric MSP-WD scenario). We may also play this game for the Galactic disk eccentric millisecond binary system PSR J1903+0327 which has an orbital period of 95 days and an eccentricity of 0.44 (Champion et al. 2008). Although not plotted in Figure 16, this system sits close to three double NS systems, perhaps suggesting that PSR J1903+0327 could also be a low mass eccentric MSP-NS binary system. The model ratio of eccentric to circular MSP systems is 0.34. This is assuming that any system with an eccentricity less than 0.001 is counted as circular. The model does not follow eccentricity evolution below 0.001 owing to concerns about accuracy, i.e. systems with eccentricities lower than this are considered to be circular.

Although not shown here directly it is possible for us to

produce MSP-BH systems. Unfortunately, all of the MSPs in these systems accrete enough material that their magnetic fields decay quickly beyond the pulsar visibility limit. However, it is interesting to see that we are able to produce rapidly rotating NSs with BH companions. A typical evolutionary formation scenario begins with two large stars, the primary  $M_1 \sim 65 M_\odot$  and secondary  $M_2 \sim 30 M_\odot$  in a close orbit separation  $a \sim 40 R_\odot$  (an orbital period of  $\sim 5$  days). Both stars begin to rapidly lose mass in winds and eventually the primary initiates mass transfer, at a system time of 2.5 Myr by which time it has already lost  $\sim 4 M_\odot$  and the companion has lost  $\sim 0.3 M_\odot$ . When the RLOF mass-transfer phase ends some 2 Myr later the primary star is now a core-helium burning star with  $8 M_\odot$  and the secondary is a  $66 M_\odot$  main sequence star. The orbit has increased to a separation of  $\sim 180 R_\odot$ . The primary star then rapidly evolves through naked helium phases to become a  $2.4 M_\odot$  NS. The system survives the SN event and is now 5.2 Myr old with a separation of  $\sim 400 R_\odot$  between the stars. The companion begins to evolve quickly off the main sequence and in the 0.5 Myrs it takes to become a  $13 M_\odot$  BH it loses  $30 M_\odot$  in a wind. The NS has accreted  $0.07 M_\odot$  of this material which is enough to spin it up to a millisecond spin period. We find that 0.8% of the binary pulsars rotating with periods less than 0.02 have a BH companion (including those that have decayed to the bottom magnetic field limit). Of these rapidly rotating NSs with BH companions just under half occur with orbital periods less than 50 days (the smallest orbital period is just under 0.1 days). Also, the majority of them (94%) have eccentricities greater than 0.2. It can be supposed that if one modifies our method for decaying the magnetic field during accretion such that (some of) the above system MSPs do not decay beyond the pulsar death line, it could be possible to produce observable MSP-BH systems in relativistic orbits (that is a heavy, tight and eccentric binary system in which one may constrain general relativity) within the Galactic disk.

## 6 DISCUSSION

In the previous sections we investigated a range of input parameters and evolutionary assumptions that affect the outcomes for isolated and binary pulsar evolution. This lead us to a preferred model which gave good coverage of the  $P\dot{P}$  parameter space. For that model we examined NS and orbital properties comparing them to observations. We next inspect some aspects of the results in further detail and comment on areas we think are important for future work.

Modelling beaming and accretion selection effects significantly reduces the number of observable pulsars predicted by our model. Within this Model Fc there was uncertainty in how to deal with Thorne-Żytkow objects. Within Section 5.6 our assumption was that the NS reset during the destruction of the TŻO (made for simplicity). At present we are unsure if this is a realistic assumption to make. If we instead assume the pulsar is unchanged when passing through a TŻO evolutionary phase we find many more isolated MSP systems are produced. Coupled to this, in Section 5.8.2, we assumed that when the material is expelled from the TŻO, leaving behind a NS, that the expelled material enshrouds the NS for long enough that it is not observed before crossing the death

line (very much like the assumption for post-accretion NSs). Again, we are unsure how physically correct this assumption is. Below are a number of other possible evolutionary assumptions that could be made when dealing with these systems. Perhaps the NS should accrete some amount of material, decaying the magnetic field, and, if enough material is accreted, form a BH (Fryer, Benz & Herant 1996). Or if a BH is not formed perhaps a revitalised NS is born (Podsiadlowski 1996) – a standard isolated pulsar, or a pulsar which is below the death line. But one may even consider an outcome that is quite interesting. That is the possible formation of a magnetar. It could even be assumed that the surrounding material causes a severe braking mechanism, the outcome of which is a young hot highly magnetic slowly-rotating NS (see below for further discussion on possible magnetar population synthesis).

We showed in Section 5.5 that values of the magnetic field decay timescale,  $\tau_B$ , below 100 Myrs do not provide a realistic distribution of pulsars. Then in Section 5.6 we explained that using  $\tau_B = 1000$  Myr does not cover enough of the slow rotating pulsars in the  $P\dot{P}$  diagram but that using  $\tau_B > 2000$  Myr over corrected for this. For our preferred model we found  $\tau_B = 2000$  Myr to be optimal. We note that the choice of maximum age for the population, in our case 10 Gyr, affects the time available for decay and as a result affects the appearance of the pulsar distribution at the lower edge of the main pulsar island. However, the appearance of this region also depends crucially on the details and/or shortcomings of the assumed death line used in the model (which we now discuss).

In all our models the recycled pulsars are not suitably limited by the death line. Of course, the inverse Compton scattered death line models have not been considered in any detail, and as Hibschan & Arons (2001) suggest all three models may be required to suitably simulate the complete pulsar population death line. In fact, Hibschan & Arons (2001) show regions of  $P\dot{P}$  in which the different methods would come into play. The standard pulsar island is shown to be modelled by CR, the recycled pulsars by nonresonant inverse Compton scatter and the high magnetic field pulsars governed by the resonant inverse Compton scattered method. This matches our findings that CR models the standard pulsar island death line in a suitable manner but is too lax in culling recycled pulsars. To test this further we now examine what effect decreasing  $\tilde{f}_{\text{prim}}^{\text{min}}$  to 0.10 (from the previously assumed 0.15) has on our pulsar population. The recycled pulsar island is now more effectively constrained by the death line. However, the death line is now too effective at culling pulsars from the standard pulsar island. As explained previously (see section 3.7), the death line is broken up into two regimes, saturated and unsaturated. Within all the models so far it seems that the majority of pulsars are constrained by the saturated death line region (even if we are to decrease  $\tilde{f}_{\text{prim}}^{\text{min}}$  to 0.03). In fact, any pulsar at the beginning of its accretion phase is governed by the saturated regime (although at some point after this it may move into the unsaturated regime for a time). To increase the influence of the unsaturated regime we can take some liberties with the assumed unsaturated  $\tilde{f}_{\text{prim}}^{\text{min}}$  value and let it approach zero. However, this eliminates a wedge of pulsars from a region of the  $P\dot{P}$  space in which pulsars are observed and this is not an acceptable parameter change. We note that death

line calculations are model dependent and in particular the assumed NS equation of state is an important feature and is something we have not considered here in any detail. Further work is required in examining all the Harding, Muslimov & Zhang (2002) death lines but is beyond the scope of this paper.

All the models presented here allow the creation of NSs with spin frequencies in excess of 1000 Hz. The only reason these NSs do not spin beyond  $\sim 3300$  Hz (see, say, Figure 10) is that, within BSE, no star is allowed to spin beyond their break-up speed. There are theoretical mechanisms that allow the regulation of pulsar spin and restrict it to some spin velocity less than the break-up velocity. One such possible mechanism is gravitational emission from the pulsar itself. There are two theories as to how a pulsar may emit gravitational radiation and thus self-regulate its own spin period. One theory suggests that if a pulsar surface is not smooth or purely spherical (this would be the case for those that have accreted material or that have strong magnetic fields and are rotating rapidly) then this asymmetry in the pulsars features may be mapped to the pulsars space time curvature and cause energy dissipation in the form of gravity waves (Shapiro & Teukolsky 1983; Bildsten 1998; Payne & Melatos 2005). The other theory assumes that the Rosby wave (r-wave or r-mode) instability (Levin 1999; Friedman & Lockitch 2001) is not damped. This instability basically arises due to the form of the wave and the speed of rotation of the pulsar. Chandrasekhar (1970) showed that Maclaurin spheroids<sup>3</sup> with uniform density, rotating uniformly are unstable to  $l = m = 2$  polar modes (i.e., those waves in which the wave front stretches from pole to pole and travels around the sphere). In a non-rotating or slow rotating star, a particular mode, the non-axisymmetric instability removes positive and negative angular momentum from the forward and backward mode respectively (Friedman & Lockitch, 2001), thus all the non-axisymmetric modes cancel out and no instability forms. In a rapidly rotating star ( $\sim$  that around the maximum observed pulsar spin rate; Levin 1999), a backward moving mode may be moving forward as observed by an inertial observer and therefore radiate away positive angular momentum – in effect increasing the mode amplitude (Friedman & Lockitch 2001). In this manner gravitational radiation drives the mode and the star spins down until the instability dies (Levin 1999).

With the suggested discovery of a pulsar with sub-millisecond period (Kaaret et al. 2007), the maximum spin rate possible for a pulsar is work we would like to consider in the future. At the forefront of this work will be contemplation of the above gravitational radiation pulsar spin-down methods. However, we wish to point out that the assumed accretion-induced magnetic field decay parameter may play an important role in determining the observed MSP spin period cut off (see Section 5.3) and is something that will need to be considered in future work.

In recent years magnetars have become a distinct subclass of the pulsar population. These systems are highly

magnetic NSs with magnetic fields of order  $10^{14} - 10^{15}$  G. Magnetar formation is not well understood, though work by Thompson & Duncan (1993) and Duncan & Thompson (1992) showed that nascent NSs which rotate rapidly ( $\lesssim 0.03$  s) can have magnetic fields within the above range. In terms of the work being completed here we have not yet considered the possibility of modeling these highly magnetised, slow rotating pulsars. The reasoning behind this is that we are trying to produce radio pulsars and these systems have only been found in X-rays (anomalous X-ray repeaters) and gamma-rays (soft gamma-ray repeaters: see Woods & Thompson 2006 for review). However, in light of the now constant flow of new and improving theoretical and observational considerations of these objects (Spruit & Phinney 1998; Heger et al. 2003; Heger, Woosley & Spruit 2005; Mezzacappa 2005; Thompson 2006; Harding & Lai 2006; Blondin & Mezzacappa 2006) an attempt to model these systems with very simple assumptions is now possible and will be included in future work.

## 7 CONCLUSIONS

We model the evolution of radio pulsars, both single and in binary systems. Models are evolved from realistic initial mass functions, period distribution and parameter ranges. Our primary goal is to demonstrate that we have an evolution algorithm that can generate the range of pulsars observed in the Galaxy, thus laying the groundwork for a synthetic Galactic population code that will ultimately include kinematics and selection effects. However, through investigation of the  $P\dot{P}$  diagram (comparing model-model and model-observation) we have already been able to demonstrate how uncertain factors of pulsar and binary evolution can be constrained. We have also been able to make preliminary predictions about the Galactic pulsar population, in particular MSPs. This represents the first study combining detailed binary evolution and pulsar physics. Of course a study such as this is hampered by many poorly constrained parameters which may result in misleading results. This is especially true if the complete relevant parameter space is not examined and multiple observations are not used as benchmarks. Therefore, we once again remind the reader that some caution is required when examining our results.

In terms of pulsar evolution it has been possible to provide constraints on various aspects of the modelling. For instance, our models can demonstrate that magnetic field decay timescales of order 100 Myr or less can not produce the required distribution of spun-up pulsars. We also show that propeller evolution has a large impact on pulsar populations and can be an important component of pulsar modelling. In particular we show that the inclusion of the propeller mechanism causes wind accretion to be the dominant pathway for MSP production. In fact, neglecting propeller evolution is necessary in order to produce any sort of RLOF disk accretion powered MSP (the typical type of observed accretion powered MSP). To further investigate this aspect there is a need to examine methods for dealing with accretion physics in more detail – including the addition of transient RLOF accretion features. We find that accretion-induced magnetic field decay (or apparent field decay) provides a natural method for forming rapidly rotating low magnetic

<sup>3</sup> A method for modeling uniform density ellipsoids. In particular it gives a description of the relationship between the eccentricity of the system, in this case the pulsar, and its uniform angular momentum.

field NSs. Without any such magnetic field decay we find there is no hope of theoretically reproducing the observed pulsar  $P\dot{P}$  distribution. The accretion-induced method assumed here works well for all models performed and we depict how changes in the efficiency of the decay modifies the populated  $P\dot{P}$  region. Including an angular momentum wind accretion efficiency parameter – lowering the angular momentum accreted – assists in producing some of the tightest observational  $P\dot{P}$  constraints. We also find that the addition of an electron capture asymmetric SN kick distribution results in the formation of a greater number of MSPs than in previous models. As such this evolutionary assumption will doubtlessly be an important feature in future works and requires further examination.

We demonstrate the predictive power of our code by examining the pulsar mass range and eccentricity of MSP systems produced in a favoured model. We must wait to impose selection effects before we can advise as to what fraction of these are potentially observable. We also show that under standard accretion physics assumptions NSs are able to accrete up to  $\sim 1 M_{\odot}$  of material, which can spin them up to rapid rotation rates and decay their magnetic fields to strengths considered insufficient for producing radio emission.

We conduct an initial investigation into how the  $P\dot{P}$  parameter space is modified when selection effects are considered. These include beaming and blanketing of the pulse by material thrown off by stellar winds or during mass accretion events. We study the distributions of primordial primary mass, secondary mass and orbital period for binaries that produce pulsars. Changes in these distributions due to assumed evolutionary variations are examined. In particular we show that close binary evolution is effective in boosting the numbers of observable pulsars. Finally, it is clear from all of our models that a greater level of detail is required when calculating the complete pulsar population death line.

The work shown here makes use of the first of three modules that will eventually be able to simulate pulsar observational surveys, including next generation radio surveys such as the Square Kilometer Array. This involves following the positions of pulsars within the Galactic gravitational potential and modelling survey selection effects. The long term aim is to include multi-wavelength survey capability into our models, and thus observe any Galactic stellar population. It is important to point out here that once complete this code will consist of the most comprehensive treatment of input physics and selection effects for pulsar simulation, something not previously attempted.

## ACKNOWLEDGMENTS

PDK wishes to thank Swinburne University of Technology for a PhD scholarship. PDK also thanks Joris Verbiest for discussions on observed pulsar masses. The authors wish to thank the referee who helped improve the focus of this work.

## REFERENCES

- Arons J., Scharlemann E.T., 1979, *ApJ*, 231, 271  
 Arzoumanian Z., Cordes J. M., Wasserman I., 1999, *ApJ*, 520, 696  
 Baade W., Zwicky F., 1934a, *Proc. Nat. Acad. Sci.*, 20, 254  
 Baade W., Zwicky F., 1934b, *Proc. Nat. Acad. Sci.*, 20, 259  
 Bailes M., 1989, *ApJ*, 324, 917  
 Belczynski K., Kalogera V., Bulik T., 2002, *ApJ*, 572, 407  
 Belczynski K., Kalogera V., Rasio F.A., Taam R.E., Zezas A., Bulik T., Maccarone T.J., Ivanova N., 2008, *ApJS*, 174, 223  
 Bell J.F., Bailes M., Bessell M.S., 1993, *Nature*, 364, 603  
 Beloborodov A.M., 1998, *MNRAS*, 297, 793  
 Bhattacharya D., 2002, *A&A*, 23, 67  
 Bhattacharya D., Wijers R.A.M.J., Hartman J.W., Verbunt F., 1992, *ApJ*, 254, 198  
 Bisnovatyi-Kogan G.S., Komberg B.V., 1974, *SvA*, 18, 217  
 Bildsten L., 1998, *ApJ*, 501, 89  
 Blondin J.M., Mezzacappa A., 2006, *ApJ*, 642, 401  
 Bonačić Marinović A.A., Glebbeek E., Pols O.R., *astro-ph/0710.4859*, accepted by *A&A*  
 Burgay M., et al., 2003, *Nature*, 426, 531  
 Burgay M., Joshi B.C., D’Amico N., Possenti A., Lyne A.G., Manchester R.N., McLaughlin M.A., Kramer M., Camilo F., Freire P.C.C., 2006, *MNRAS*, 368, 283  
 Cameron A.G.W., Mock M., 1967, *Nature*, 215, 464  
 Champion D.J., et al., 2008, in Bassa C.G., Wang Z., Cumming A., Kaspi V.M., eds., *AIP Conf. Ser. Vol. 938*, 40  
 Years of Pulsars – Millisecond Pulsars, Magnetars, and More, American Inst. of Physics, New York, p. 448  
 Chandrasekhar S., 1970, *ApJ*, 161, 561  
 Chen K., & Ruderman M., 1993, *ApJ*, 402, 246  
 Choudhuri A.R., Konar S., 2002, *MNRAS*, 332, 933  
 Choudhuri A.R., Konar S., 2004, *Curr. Sci.*, 86, 444  
 Colpi M., Possenti A., Popov S., Pizzolato F., 2001, *LNP*, 578, 440  
 Contopoulos I., Spitkovsky A., 2006, *ApJ*, 643, 1139  
 Cumming A., Zweibel E., Bildsten L., 2001, *ApJ*, 557, 958  
 Dai H., Liu X., Li X., 2006, *ApJ*, 653, 1410  
 Davidson K., Ostriker J.P., 1973, *ApJ*, 179, 585  
 Deloye C.J., 2007, *astro-ph/0710.0189*  
 Dewey R.J., Cordes J.M., 1987, *ApJ*, 321, 780  
 Dewi J. D. M., Tauris T. M., 2001, in Podsiadlowski P., Rappaport S., King A. R., D’Antona F., Burderi L., eds., *ASP Conf. Ser. Vol. 229*, Evolution of Binary and Multiple Star Systems. Astron. Soc. Pac., San Francisco, p. 255  
 Dewi J.D.M., van den Heuvel E.P.J., 2004, *MNRAS*, 349, 169  
 Dewi J.D.M., Podsiadlowski P., Pols O.R., 2005, *MNRAS*, 363, 71  
 Duncan R.C., Thompson C., 1992, *ApJ*, 392, 9  
 Duquennoy A., Mayor M., 1991, *A&A*, 248, 485  
 Faucher-Giguere C., Kaspi V.M., 2006, *ApJ*, 643, 332  
 Faulkner A.J., et al., 2005, *ApJ*, 618L, 119  
 Ferrario L., Wickramasinghe D., 2007, *MNRAS*, 375, 1009  
 Freire P.C.C., Gupta Y., Ransom S.M., Ishwara-Chandra C. H., 2004, *ApJ*, 606, L53  
 Freire P.C.C., 2007, *astro-ph/0712.0024*  
 Freire P.C.C., Ransom S.M., Gupta Y., 2007, *ApJ*, 662, 1177  
 Friedman S.L., Lockitch K.H., 2001, in Gurzadyan V., Jantzen R., Ruffini R., eds., *Proc. Ninth Marcel Gross-*

- man Meeting on General Relativity. World Scientific, Singapore, p. 163
- Fryer C.L., Benz W., Herant M., 1996, *ApJ*, 460, 801
- Fryer C.L., 1999, *ApJ*, 522, 413
- Fryer C.L., Kalogera V., 2001, *ApJ*, 545, 548
- Fryer C.L., Young P.A., 2007, *ApJ*, 664, 1033
- Galloway D.K., 2007, *ASPC*, 362, 105
- Geppert U., Urpin V., 1994, *MNRAS*, 271, 490
- Gold T., 1968, *Nature*, 218, 731
- Goldreich P., Julian W.H., 1969, *ApJ*, 157, 869
- Gonthier P.L., Ouellette M.S., Berrier J., O'Brien S., Harding A.K., 2002, *ApJ*, 565, 482
- Gonthier P.L., Van Guilder R., Harding A.K., 2004, *ApJ*, 604, 775
- Gotthelf E.V., Halpern J.P., 2007, *astro-ph/0704.2255*
- Gunn J.E., Ostriker J.P., 1970, *ApJ*, 160, 979
- Harding A.K., Contopoulos I., Kasanas D., 1999, *ApJ*, 525, 125
- Harding A.K., Lai D., 2006, *RPPh.*, 69, 263
- Harding A.K., Muslimov A.G., 1998, *ApJ*, 508, 328
- Harding A.K., Muslimov A.G., 2001, *ApJ*, 556, 987
- Harding A.K., Muslimov A.G., 2002, *ApJ*, 568, 862
- Harding A.K., Muslimov A.G., Zhang B., 2002, *ApJ*, 576, 375
- Hartman J.M., Bhattacharya D., Wijers R., Verbunt F., 1997, *A&A*, 322, 477
- Heger A., Fryer C.L., Woosley S.E., Langer N., Hartmann D.H., 2003, *ApJ*, 591, 288
- Heger A., Woosley S.E., Spruit H.C., 2005, *ApJ*, 626, 350
- Herant M., Benz W., Colgate S.A., 1992, *ApJ*, 395, 642
- Herant M., Benz W., Hix R.W., Fryer C.L., Colgate S.A., 1994, *ApJ*, 435, 334
- Hewish A., Bell J.S., Pilkington J.D., Scott P.F., Collins R.A., 1968, *Nature*, 217, 709
- Hibschman J.A., Arons J., *ApJ*, 554, 624
- Hobbs G., Lorimer D.R., Lyne A.G., Kramer M., 2005, *MNRAS*, 360, 974
- Huang H., Becker W., 2007, *astro-ph/071611*
- Hurley J.R., Pols O.R., Tout C.A., 2000, *MNRAS*, 315, 543
- Hurley J.R., Tout C.A., Pols O.R., 2002, *MNRAS*, 329, 897
- Illarionov A.F., Sunyaev R.A., 1975, *A&A*, 39, 185
- Ivanova N., Heinke C., Rasio F.A., Belczynski K., Fregeau J., 2007, *astro-ph/0706.4096*
- Jahan-Miri M., Bhattacharya D., 1994, *MNRAS*, 269, 455
- Jahan-Miri M., 2000, *ApJ*, 532, 514
- Janka H.-Th., Langanke K., Marek A., Martinez-Pinedo G., Muller B., 2006, *astro-ph/0612072*
- Kaaret et al., 2007, *ApJ*, 657, 97
- Kalogera V., Webbink R.F., 1998, *ApJ*, 493, 351
- Kiel P.D., Hurley J.R., 2006, *MNRAS*, 369, 1152
- Kim C., Kalogera V., Lorimer D.R., 2003, *ApJ*, 584, 485
- Kitaura F.S., Janka T.H., Hillebrandt W., 2006, *A&A*, 450, 345
- Konar S., Bhaattacharya D., 1997, *MNRAS*, 284, 311
- Konar S., Bhaattacharya D., 1999a, *MNRAS*, 303, 588
- Konar S., Bhaattacharya D., 1999b, *MNRAS*, 308, 795
- Konar S., Choudhuri A.R., 2004, *MNRAS*, 348, 661
- Krimm H.A., et al., 2007, *ApJ*, 668, 147
- Kroupa P., Tout C.A., Gilmore G., 1993, *MNRAS*, 262, 545
- Kulkarni A.K., Romanova M.M., 2008, *astro-ph/0802.1759*
- Kundt W., 1976, *Phys. Letters*, 57A, 195
- Kuranov A.G., Postnov K.A., 2006, *AstL*, 32, 393
- Lattimer J.M., Prakash M., 2007, *Phys. Rep.*, 422, 109
- Levin Y., 1999, *ApJ*, 517, 328
- Lorimer D.R., Bailes M., Dewey R.J., Harrison P.A., 1993, *MNRAS*, 263, 403
- Lorimer D.R., Bailes M., Harrison P.A., 1997, *MNRAS*, 289, 592
- Lorimer D.R., 2007, *Nature*, 428, 900
- Lovelace R.V.E., Romanova M.M., Bisnovatyi-Kogan G.S., 2005, *ApJ*, 625, 957
- Liu X.-W., Lai X.-D., 2006, *A&A*, 446, 135
- Lyne A.G., Manchester R.N., Taylor J.H., 1985, *MNRAS*, 213, 613
- Lyne A.G., Lorimer D.R., 1994, *Nature*, 369, 127
- Lyne A.G., et al., 2004, *Science*, 303, 1153
- Manchester R.N., Hobbs G.B., Teoh A., Hobbs M., 2005, *ApJ*, 129, 1993
- Marek A., Janka T.H., 2007, *astro-ph/0708.3372*
- Melatos A., Payne D.J.B., 2005, *ApJ*, 623, 1044
- Melatos A., Phinney E.S., 2001, *PASA*, 18, 421
- Mezzacappa A., Blondin J.M., 2003, in Hillebrandt W., Leibundgut B., eds., Springer-Verlag, p.63
- Mezzacappa A., 2005, *ARNPS*, 55, 467
- Mezzacappa A., Bruenn S.W., Blondin J.M., Hix R.W., Messer B.O.E., 2007, *AIPC*, 942, 234
- Michel F.C., 1987, *Nature*, 329, 310
- Miyaji S., Nomoto K., Yokoi K., Sugimoto D., 1980, *PASJ*, 32, 303
- Muslimov A.G., Tsygan A.I., 1985, *Ap&SS*, 115, 43
- Muslimov A.G., Tsygan A.I., 1992, *MNRAS*, 255, 61
- Nice D.J., 2006, *Adv. S.R.*, 38, 2721
- Nice D.J., Stairs I.H., Kasian L.E., 2008, in Bassa C.G., Wang Z., Cumming A., Kaspi V.M., *AIP Conf. Ser. Vol. 938, 40 Years of Pulsars – Millisecond Pulsars, Magnetars, and More*, Americal Inst. of Physics, New York, p. 453
- Nomoto K., 1984, *ApJ*, 277, 791
- Nomoto K., 1987, *ApJ*, 322, 206
- Nomoto K., Kondo Y., 1991, *ApJ*, 367L, 19
- O'Shaughnessy R., Kim C., Fragos T., Kalogera V., Belczynski K., 2005, *ApJ*, 633, 1076
- O'Shaughnessy R., Kim C., Kalogera V., Belczynski K., 2008, *ApJ*, 672, 479
- Ostriker J.P., Gunn J.E., 1969, *ApJ*, 157, 1395
- Pacini F., 1967, *Nature*, 216, 567
- Payne D.J.B., Melatos A., 2004, *MNRAS*, 351, 569
- Payne D.J.B., Melatos A., 2005, *ApJ*, 623, 1044
- Pfahl E., Rappaport S., Podsiadlowski P., 2002, *ApJ*, 571, 37
- Pfahl E., Rappaport S., Podsiadlowski P., Spruit H., 2002, *ApJ*, 574, 364
- Phinney E.S., Blandford R.D., 1981, *MNRAS*, 194, 137
- Podsiadlowski P., 1996, in van Paradijs J., van den Heuvel E.P.J., Kuulkers E., eds., *IAUS*, 165, *Compact Stars in Binaries*, Kluwer Academic publishers, Dordrecht, p. 29
- Podsiadlowski P., Rappaport S., Han Z., 2003, *MNRAS*, 341, 385
- Podsiadlowski P., Langer N., Poelarends A.J.T., Rappaport S., Heger A., Pfahl E., 2004, *ApJ*, 612, 1044
- Poelarends A.J.T., Herwig F., Langer N., Heger A., 2007, *astro-ph/0705.4643*
- Portegies Zwart S.F., Verbunt F., Ergma E., 1997, *A&A*, 321, 207
- Portegies Zwart S.F., Yungelson A., 1998, *A&A*, 372, 173

- Possenti A., Colpi M., D'Amico N., Burderi L., 1998, *ApJ*, 497, L97
- Possenti A., Colpi M., Geppert U., Burderi L., D'Amico N., 1999, *ApJ*, 497, L97
- Press W.H., Teukolsky S.A., Vetterling W.T., Flannery B.P., 1992, *Numerical Recipes in FORTRAN*, 2nd ed. Cambridge University Press, Cambridge
- Pringle J.E., Rees M.J., 1972, *A&A*, 21, 1
- Rathnasree N., 1993, *MNRAS*, 260, 717
- Regimbau T., de Freibas Pacheco J.A., 2000, *A&A*, 376, 381
- Regimbau T., de Freibas Pacheco J.A., 2001, *A&A*, 374, 182
- Romani R.W., 1990, *Nature*, 347, 741
- Ruderman M., Sutherland P.G., 1975, *ApJ*, 196, 51
- Ruderman M., 1991a, *ApJ*, 366, 261
- Ruderman M., 1991b, *ApJ*, 382, 576
- Ruderman M., 1991c, *ApJ*, 382, 587
- Ruffert M., 1999, *A&A*, 346, 861
- Savonije G.J., van den Heuvel E.P.J., 1977, *ApJ*, 214, L19
- Shapiro S.L., Teukolsky S.A., 1983, *Black Holes, White Dwarfs, and Neutron Stars* (New York: Wiley-Interscience)
- Shibazaki N., Murakami T., Shaham J., Nomoto K., 1989, *Nature*, 342, 656
- Shklovsky I.S., 1970, *SvA*, 13, 562
- Spitkovsky A., 2006, *astro-ph/0603147*
- Spruit H.C., Phinney E.S., 1998, *Nature*, 393, 139
- Stollman G.M., 1987, *A&A*, 178, 143
- Story S.A., Gonthier P.L., Harding A.K., 2007, *ApJ*, 671, 713
- Taam R.E., van den Heuvel E.P.J., 1986, *ApJ*, 305, 235
- Tauris T.M., Manchester R.N., 1998, *MNRAS*, 298, 625
- Tavani M., 1992, *A&A*, 261, 472
- Taylor J.H., Manchester R.N., 1977, *ApJ*, 215, 885
- Thompson C., Duncan R.C., 1993, *ApJ*, 408, 194
- Thompson C., 2006, *ApJ*, 651, 333
- Thorne K.S., Żytkow A.N., 1977, *ApJ*, 212, 832
- Tolman R.C., 1939, *PhRv*, 55, 364
- Ulrich R.K., Burger H.L., 1976, *ApJ*, 206, 509
- Urpin V., Geppert U., 1995, *MNRAS*, 275, 1117
- Urpin V., Geppert U., Konenkov, D. 1997, *MNRAS*, 292, 167
- van den Heuvel E.P.J., 1984, *A&A*, 5, 209
- van den Heuvel E.P.J., 2007, *astro-ph/0704.1215*
- van Kerkwijk M.H., Bassa C.G., Jocoby B.A., Jonker P.G., 2004, in Rasio F.A., Stairs I.H., eds, *ASP Conf. Ser. Vol. 328, Binary Radio Pulsars*, Astron. Soc. Pac., San Francisco, p.357
- van Paradijs J., Allington-Smith J., Callanan P., Hassall B.J.M. & Charles P.A., 1988, *Nature*, 334, 684
- van Straten W., Bailes M., Britton M., Kulkarni S.R., Anderson S.B., Manchester R.N., Sarkissian J., *Nature*, 412, 158
- Verbiest J.P.W., et al., 2008, accepted by *ApJ*, *astro-ph/0801.2589*
- Vivekanand M., Narayan R., 1981, *JA&A*, 2, 315
- Wheeler J.A., 1966, *Ann. Rev. Astr. and Ap.*, 4, 393
- Willems B., Kolb U., 2002, *MNRAS*, 337, 1004
- Winkler C., 2007, *astro-ph/0712.0470*
- Woods P.M., Thompson C., 2006, in Lewin W.H.G., van der Klis, eds. *Cambridge, U.K.*, p.547
- Zhang B., Harding A.K., Muslimov A.G., 2000, *ApJ*, 531, L135
- Zhang C.M., Kojima Y., 2006, *MNRAS*, 366, 137

This paper has been typeset from a  $\text{\TeX}$ / $\text{\LaTeX}$  file prepared by the author.